Implicit Regularization in Nonconvex Statistical Estimation: Gradient Descent Converges Linearly for Phase Retrieval, Matrix Completion and Blind Deconvolution

Cong Ma* Kaizheng Wang* Yuejie Chi† Yuxin Chen‡

November 2017

Abstract

Nonconvex optimization algorithms are provably efficient for solving many statistical estimation problems. Due to the highly nonconvex nature of the empirical loss, state-of-the-art results often require proper regularization procedures (e.g. trimming, regularized cost, projection) in order to guarantee fast convergence. For vanilla procedures such as gradient descent, however, prior theory either recommends highly conservative step sizes to avoid overshooting, or completely lacks performance guarantees.

This paper uncovers a striking phenomenon in nonconvex optimization: even in the absence of explicit regularization, gradient descent enforces proper regularization implicitly under various statistical models. In fact, gradient descent follows a trajectory that always falls within a basin incoherent with the measurement mechanism — a region that enjoys nice geometry. This "implicit regularization" feature allows the algorithm to proceed in a far more aggressive fashion without overshooting, which in turn results in a near-optimal convergence rate and substantial computational savings. Focusing on three fundamental statistical estimation problems, i.e. phase retrieval, low-rank matrix completion, and blind deconvolution, we establish that gradient descent achieves near-optimal statistical and computational guarantees without explicit regularizations. In particular, by marrying statistical modeling with generic optimization theory, we propose a general recipe for analyzing the trajectories of iterative algorithms via a leave-one-out perturbation argument, which might be of independent interest.

Contents

*Department of Operations Research and Financial Engineering, Princeton University, Princeton, NJ 08544, USA; Email: {congm, kaizheng}@princeton.edu.

†Department of Electrical and Computer Engineering, The Ohio State University, Columbus, OH 43210, USA; Email: chi.97@osu.edu.

‡Department of Electrical Engineering, Princeton University, Princeton, NJ 08544, USA; Email: yuxin.chen@princeton.edu.

1 Introduction

1.1 Nonlinear systems of equations and empirical loss minimization

A wide spectrum of science and engineering applications calls for solutions to a nonlinear system of equations. Imagine we have collected a set of data points $\boldsymbol{y} = \{y_j\}_{j=1}^m$, generated by a nonlinear sensing system,

$$y_j \approx \mathcal{A}_j\big(\boldsymbol{x}^\natural\big), \quad 1 \le j \le m,$$

where $\boldsymbol{x}^\natural$ is the unknown object of interest, and the $\mathcal{A}_j$'s are certain nonlinear maps known *a priori*. Can we reconstruct the underlying object $\boldsymbol{x}^\natural$ in a faithful yet efficient manner? Problems of this kind abound in information and statistical science, prominent examples including low-rank matrix recovery [KMO10a, CR09], robust principal component analysis [CSPW11, CLMW11], phase retrieval [CSV13, JEH15], neural networks [SJL17, ZSJ+17], to name just a few.

In principle, it is possible to attempt reconstruction by searching for a solution that minimizes the empirical loss, namely,

$$\text{minimize}_{\boldsymbol{x}} \quad f(\boldsymbol{x}) = \sum_{j=1}^m \big|y_j - \mathcal{A}_j(\boldsymbol{x})\big|^2. \tag{1}$$

Unfortunately, this empirical loss minimization problem is in many cases nonconvex, making it NP-hard in general. This issue of non-convexity comes up in, for example, several representative problems that epitomize the structures of nonlinear systems encountered in practice.[1]

- **Phase retrieval / solving quadratic systems of equations.** Imagine we are asked to recover an unknown object $\boldsymbol{x}^\natural \in \mathbb{R}^n$, but we are only given the square modulus of certain linear measurements about the object, with all sign/phase information of the measurements missing. This arises, for example, in X-ray crystallography [CESV13], and in other latent-variable models where the hidden variables are captured by the missing signs [CYC14]. To fix ideas, assume we would like to solve for $\boldsymbol{x}^\natural \in \mathbb{R}^n$ in the following quadratic system of m equations

$$y_j = \big(\boldsymbol{a}_j^\top \boldsymbol{x}^\natural\big)^2, \qquad 1 \le j \le m,$$

where $\boldsymbol{a}_j \in \mathbb{R}^n$ is the known design vector. One strategy is thus to solve the following problem

$$\text{minimize}_{\boldsymbol{x}\in\mathbb{R}^n} \quad f(\boldsymbol{x}) = \frac{1}{4m}\sum_{j=1}^m \Big[y_j - \big(\boldsymbol{a}_j^\top \boldsymbol{x}\big)^2\Big]^2. \tag{2}$$

- **Low-rank matrix completion.** In many scenarios such as collaborative filtering, we wish to make predictions about all entries of an (approximately) low-rank matrix $\boldsymbol{M}^\natural \in \mathbb{R}^{n\times n}$ (e.g. a matrix consisting of users' ratings about many movies), yet we are only revealed a highly incomplete subset of entries of $\boldsymbol{M}^\natural$ [CR09]. For clarity of presentation, assume $\boldsymbol{M}^\natural$ to be rank-r ($r \ll n$) and positive semidefinite (PSD), i.e. $\boldsymbol{M}^\natural = \boldsymbol{X}^\natural \boldsymbol{X}^{\natural\top}$ with $\boldsymbol{X}^\natural \in \mathbb{R}^{n\times r}$, and suppose we have only seen the entries

$$Y_{j,k} = M_{j,k}^\natural = (\boldsymbol{X}^\natural \boldsymbol{X}^{\natural\top})_{j,k}, \qquad (j,k) \in \Omega$$

within some index subset Ω of cardinality m. These entries can be viewed as nonlinear measurements about the low-rank factor $\boldsymbol{X}^\natural$. The task of completing the true matrix $\boldsymbol{M}^\natural$ can then be cast as solving

$$\text{minimize}_{\boldsymbol{X}\in\mathbb{R}^{n\times r}} \quad f(\boldsymbol{X}) = \frac{n^2}{4m}\sum_{(j,k)\in\Omega} \big(Y_{j,k} - \boldsymbol{e}_j^\top \boldsymbol{X}\boldsymbol{X}^\top \boldsymbol{e}_k\big)^2, \tag{3}$$

where the $\boldsymbol{e}_j$'s stand for the canonical basis vectors in $\mathbb{R}^n$.

[1] Here, we choose different pre-constants in front of the empirical loss in order to be consistent with the literature of the respective problems.

- **Blind deconvolution / solving bilinear systems of equations.** Imagine we are interested in estimating two signals of interest $\boldsymbol{h}^\natural, \boldsymbol{x}^\natural \in \mathbb{C}^K$, but we only collect a few bilinear measurements about them. This problem arises from mathematical modeling of *blind deconvolution* [ARR14, LLSW16], which frequently arises in astronomy, imaging, communications, etc. The goal is to recover two signals from their convolution. Put more formally, suppose we have acquired m bilinear measurements taking the following form
$$y_j = \boldsymbol{b}_j^* \boldsymbol{h}^\natural \boldsymbol{x}^{\natural *} \boldsymbol{a}_j, \qquad 1 \le j \le m,$$
where $\boldsymbol{a}_j, \boldsymbol{b}_j \in \mathbb{C}^K$ are distinct design vectors (e.g. Fourier and/or random design vectors) known *a priori*. In order to reconstruct the underlying signals, one asks for solutions to the following problem
$$\text{minimize}_{\boldsymbol{h},\boldsymbol{x}\in\mathbb{C}^K} \quad f(\boldsymbol{h},\boldsymbol{x}) = \sum_{j=1}^m \left| y_j - \boldsymbol{b}_j^* \boldsymbol{h}\boldsymbol{x}^* \boldsymbol{a}_j \right|^2.$$

1.2 Nonconvex optimization via regularized gradient descent

First-order methods have been a popular heuristic in practice for solving nonconvex problems including (1). For instance, a widely adopted procedure is gradient descent following the update rule
$$\boldsymbol{x}^{t+1} = \boldsymbol{x}^t - \eta_t \nabla f\big(\boldsymbol{x}^t\big), \qquad t \ge 0, \tag{4}$$
where η_t is the step size (or learning rate) and $\boldsymbol{x}^0$ is some proper initial guess. Given that it only performs a single gradient calculation $\nabla f(\cdot)$ per iteration (which typically can be completed within near-linear time), this paradigm emerges as a candidate for solving large-scale problems. The concern is: whether $\boldsymbol{x}^t$ converges to the global solution and, if so, how long it takes for convergence, especially since (1) is highly nonconvex.

Despite the worst-case hardness, fortunately, appealing convergence properties have been discovered in various statistical estimation problems; the blessing being that the statistical models help rule out ill-behaved instances. For the average case, the empirical loss often enjoys benign geometry, in a *local* region (or at least along certain directions) surrounding the global optimum. In light of this, an effective nonconvex iterative method typically consists of two stages:

1. a carefully-designed initialization scheme (e.g. spectral method);
2. an iterative refinement procedure (e.g. gradient descent).

This strategy has recently spurred a great deal of interest, owing to its promise of achieving computational efficiency and statistical accuracy at once for a glowing list of problems (e.g. [KMO10a, JNS13, CW15, SL16, CLS15, CC17, LLSW16, LLB17]). However, rather than directly applying gradient descent (4), existing theory often suggests enforcing proper regularization. Such explicit regularization enables improved computational convergence by properly "stabilizing" the search directions. The following regularization schemes, amongst others, have been suggested to obtain or improve computational guarantees. We refer to these algorithms collectively as *Regularized Gradient Descent*.

- *Trimming/truncation*, which discards/truncates a subset of the gradient components when forming the descent direction. For instance, when solving quadratic systems of equations, one can modify the gradient descent update rule as
$$\boldsymbol{x}^{t+1} = \boldsymbol{x}^t - \eta_t \mathcal{T}\left(\nabla f\big(\boldsymbol{x}^t\big)\right), \tag{5}$$
where $\mathcal{T}$ is an operator that effectively drops samples bearing too much influence on the search direction. This strategy [CC17, ZCL16, WGE17] has been shown to enable exact recovery with linear-time computational complexity.
- *Regularized loss*, which attempts to optimize a regularized empirical risk
$$\boldsymbol{x}^{t+1} = \boldsymbol{x}^t - \eta_t \left(\nabla f\big(\boldsymbol{x}^t\big) + \nabla R\big(\boldsymbol{x}^t\big)\right), \tag{6}$$
where $R(\boldsymbol{x})$ stands for an additional penalty term in the empirical loss. For example, in low-rank matrix completion [KMO10a, SL16], $R(\cdot)$ imposes penalty based on the ℓ_2 row norm of the decision matrix, while in blind deconvolution [LLSW16, HH17, LS17], it penalizes the ℓ_2 norm as well as certain component-wise incoherence measure of the decision vectors.

Table 1: Prior theory for gradient descent (with spectral initialization)

	Vanilla gradient descent			Regularized gradient descent		
	sample complexity	iteration complexity	step size	sample complexity	iteration complexity	type of regularization
Phase retrieval	$n \log n$	$n \log \frac{1}{\epsilon}$	$1/n$	n	$\log \frac{1}{\epsilon}$	trimming [CC17, ZCL16]
Matrix completion	n/a	n/a	n/a	nr^7	$\frac{n}{r} \log \frac{1}{\epsilon}$	regularized loss [SL16]
				nr^2	$r^2 \log \frac{1}{\epsilon}$	projection [CW15, ZL16]
Blind deconvolution	n/a	n/a	n/a	$K \text{poly} \log m$	$m \log \frac{1}{\epsilon}$	regularized loss & projection [LLSW16]

- *Projection*, which projects the iterates onto certain sets based on prior knowledge, that is,

$$\boldsymbol{x}^{t+1} = \mathcal{P}\left(\boldsymbol{x}^t - \eta_t \nabla f\left(\boldsymbol{x}^t\right)\right), \tag{7}$$

  where $\mathcal{P}$ is a certain projection operator used to enforce, for example, incoherence properties. This strategy has been employed in both low-rank matrix completion [CW15, ZL16] and blind deconvolution [LLSW16].

Equipped with such regularization procedures, existing works uncover appealing computational and statistical properties under various statistical models. Table 1 summarizes the performance guarantees derived in the prior literature; for simplicity, only orderwise results are provided.

Remark 1. There is another role of regularization commonly studied in the literature, which exploits prior knowledge about the structure of the unknown object — a procedure that is particularly important in preventing overfitting and improving statistical generalization. This is, however, not the focal point of this paper, since we are primarily pursuing solutions to (1) without imposing additional structure.

1.3 Regularization-free procedures?

The regularized gradient descent algorithms, while exhibiting appealing performance, usually introduce more algorithmic parameters that need to be carefully tuned based on the assumed statistical models. In contrast, vanilla gradient descent (cf. (4)) — which is perhaps the very first method that comes into mind and requires minimal tuning parameters — is far less understood (cf. Table 1). Take matrix completion and blind deconvolution as examples: to the best of our knowledge, there is currently no theoretical guarantee derived for unregularized gradient descent.[2]

The situation is better for phase retrieval: the local convergence of vanilla gradient descent, also known as Wirtinger flow (WF), has been investigated in [CLS15, WWS15]. Under i.i.d. Gaussian design and with near-minimal sample complexity, WF (combined with spectral initialization) provably achieves ϵ-accuracy (in a relative sense) within $O\big(n \log \frac{1}{\epsilon}\big)$ iterations. Nevertheless, the computational guarantee is significantly outperformed by the regularized version (called truncated Wirtinger flow [CC17]), which only requires $O\big(\log \frac{1}{\epsilon}\big)$ iterations to converge with similar per-iteration cost. On closer inspection, the high computational cost of WF is largely due to the vanishingly small step size $\eta_t = O\big(\frac{1}{n\|\boldsymbol{x}^\natural\|_2^2}\big)$ — and hence slow movement — suggested by the theory [CLS15]. While this is already the largest possible step size allowed in the theory published in [CLS15], it is considerably more conservative than the choice $\eta_t = O\big(\frac{1}{\|\boldsymbol{x}^\natural\|_2^2}\big)$ theoretically justified for the regularized version [CC17, ZCL16].

The lack of understanding and suboptimal results about vanilla gradient descent raise a very natural question: are regularization-free iterative algorithms inherently suboptimal when solving nonconvex statistical estimation problems of this kind?

[2] We note that the global landscape of the matrix completion problem has been studied in [GLM16], but this is also accomplished using a regularized cost function.

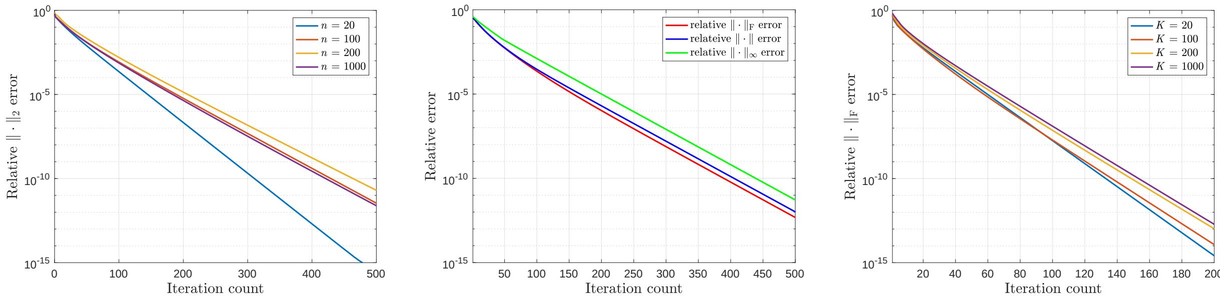

(a) phase retrieval (b) matrix completion (c) blind deconvolution

Figure 1: (a) Relative ℓ_2 error of $\boldsymbol{x}^t$ (modulo the global phase) vs. iteration count for phase retrieval under i.i.d. Gaussian design, where $m = 10n$ and $\eta_t = 0.1$. (b) Relative error of $\boldsymbol{X}^t\boldsymbol{X}^{t\top}$ (measured by $\|\cdot\|_{\mathrm{F}}, \|\cdot\|, \|\cdot\|_\infty$) vs. iteration count for matrix completion, where $n = 1000$, $r = 10$, $p = 0.1$, and $\eta_t = 0.2$. (c) Relative error of $\boldsymbol{h}^t\boldsymbol{x}^{t*}$ (measured by $\|\cdot\|_{\mathrm{F}}$) vs. iteration count for blind deconvolution, where $m = 10K$ and $\eta_t = 0.5$.

1.4 Numerical surprise of unregularized gradient descent

To answer the preceding question, it is perhaps best to first collect some numerical evidence. In what follows, we test the performance of vanilla gradient descent for phase retrieval, matrix completion, and blind deconvolution, using a *constant* step size. For all of these experiments, the initial guess is obtained by means of the standard spectral method. Our numerical findings are as follows:

- *Phase retrieval.* For each n, set $m = 10n$, take $\boldsymbol{x}^\natural \in \mathbb{R}^n$ to be a random vector with unit norm, and generate the design vectors $\boldsymbol{a}_j \overset{\text{i.i.d.}}{\sim} \mathcal{N}(\boldsymbol{0}, \boldsymbol{I}_n)$, $1 \le j \le m$. Figure 1(a) illustrates the relative ℓ_2 error $\min\{\|\boldsymbol{x}^t - \boldsymbol{x}^\natural\|_2, \|\boldsymbol{x}^t + \boldsymbol{x}^\natural\|_2\}/\|\boldsymbol{x}^\natural\|_2$ (modulo the unrecoverable global phase) vs. the iteration count. The results are shown for $n = 20, 100, 200, 1000$, with the step size taken to be $\eta_t = 0.1$ in all settings.

- *Matrix completion.* Generate an $n \times n$ random matrix $\boldsymbol{M}^\natural \succeq \boldsymbol{0}$ with dimension $n = 1000$, rank $r = 10$, and all nonzero eigenvalues equal to one. Each entry of $\boldsymbol{M}^\natural$ is observed independently with probability $p = 0.1$. Figure 1(b) plots the relative error $|||\boldsymbol{X}^t\boldsymbol{X}^{t\top} - \boldsymbol{M}^\natural|||/|||\boldsymbol{M}^\natural|||$ vs. the iteration count, where $|||\cdot|||$ can either be the Frobenius norm $\|\cdot\|_{\mathrm{F}}$, the spectral norm $\|\cdot\|$, or the entrywise ℓ_∞ norm $\|\cdot\|_\infty$. Here, we pick the step size as $\eta_t = 0.2$.

- *Blind deconvolution.* For each $K \in \{20, 100, 200, 1000\}$ and $m = 10K$, generate the design vectors $\boldsymbol{a}_j \sim \mathcal{N}(\boldsymbol{0}, \frac{1}{2}\boldsymbol{I}_K) + i\mathcal{N}(\boldsymbol{0}, \frac{1}{2}\boldsymbol{I}_K)$ for $1 \le j \le m$ independently,[3] and the $\boldsymbol{b}_j$'s are drawn from a partial Discrete Fourier Transform (DFT) matrix (to be described in Section 3.3). The underlying signals $\boldsymbol{h}^\natural, \boldsymbol{x}^\natural \in \mathbb{C}^K$ are produced as random vectors with unit norm. Figure 1(c) plots the relative error $\|\boldsymbol{h}^t\boldsymbol{x}^{t*} - \boldsymbol{h}^\natural\boldsymbol{x}^{\natural *}\|_{\mathrm{F}}/\|\boldsymbol{h}^\natural\boldsymbol{x}^{\natural *}\|_{\mathrm{F}}$ vs. the iteration count, with the step size taken to be $\eta_t = 0.5$ in all settings.

In all of these numerical experiments, vanilla gradient descent seems to enjoy remarkable linear convergence, always yielding an accuracy of 10^{-5} (in a relative sense) within around 200 iterations. In particular, for the phase retrieval problem, the step size is taken to be $\eta_t = 0.1$ although we vary the problem size from $n = 20$ to $n = 1000$. The consequence is that the convergence rates experience little changes when the problem sizes vary. In comparison, the theory published in [CLS15] seems overly pessimistic, as it suggests a diminishing step size inversely proportional to n and, as a result, an iteration complexity that worsens as the problem size grows.

In short, the above empirical results are surprisingly positive yet puzzling. Why was the computational efficiency of vanilla gradient descent unexplained or substantially underestimated in prior theory?

[3]Here and throughout, i represents the imaginary unit.

Table 2: Prior theory vs. our theory for vanilla gradient descent (with spectral initialization)

	Prior theory			Our theory		
	sample complexity	iteration complexity	step size	sample complexity	iteration complexity	step size
Phase retrieval	$n \log n$	$n \log \frac{1}{\varepsilon}$	$1/n$	$n \log n$	$\log n \log \frac{1}{\varepsilon}$	$1/\log n$
Matrix completion	n/a	n/a	n/a	$nr^3 \mathrm{poly} \log n$	$\log \frac{1}{\epsilon}$	1
Blind deconvolution	n/a	n/a	n/a	$K \mathrm{poly} \log m$	$\log \frac{1}{\epsilon}$	1

1.5 This paper

The main contribution of this paper is towards demystifying the "unreasonable" effectiveness of regularization-free nonconvex iterative methods. As asserted in previous work, regularized gradient descent succeeds by properly enforcing/promoting certain incoherence conditions throughout the execution of the algorithm. In contrast, we discover that

> *Vanilla gradient descent automatically forces the iterates to stay incoherent with the measurement mechanism, thus implicitly regularizing the search directions.*

This "implicit regularization" phenomenon is of fundamental importance, suggesting that vanilla gradient descent proceeds as if it were properly regularized. This explains the remarkably favorable performance of unregularized gradient descent in practice. Focusing on the three representative problems mentioned in Section 1.1, our theory guarantees both statistical and computational efficiency of vanilla gradient descent under random designs and spectral initialization. With near-optimal sample complexity, to attain ϵ-accuracy,

- **Phase retrieval (informal)**: vanilla gradient descent converges in $O\big(\log n \log \frac{1}{\epsilon}\big)$ iterations;
- **Matrix completion (informal)**: vanilla gradient descent converges in $O\big(\log \frac{1}{\epsilon}\big)$ iterations;
- **Blind deconvolution (informal)**: vanilla gradient descent converges in $O\big(\log \frac{1}{\epsilon}\big)$ iterations.

In words, gradient descent provably achieves (nearly) linear convergence in all of these examples. Throughout this paper, an algorithm is said to *converge (nearly) linearly* to $\boldsymbol{x}^\natural$ if the iterates $\{\boldsymbol{x}^t\}$ obey

$$\mathrm{dist}(\boldsymbol{x}^{t+1}, \boldsymbol{x}^\natural) \leq (1-c)\, \mathrm{dist}(\boldsymbol{x}^t, \boldsymbol{x}^\natural), \qquad \forall t \geq 0$$

for some $0 < c \leq 1$ that is (almost) independent of the problem size. Here, $\mathrm{dist}(\cdot,\cdot)$ can be any appropriate metric used to assess the estimation error.

As a byproduct of our theory, gradient descent also provably controls the *entrywise* empirical risk uniformly across all iterations; for instance, this implies that vanilla gradient descent controls entrywise prediction error for the matrix completion task. Precise statements of these results are deferred to Section 3 and are briefly summarized in Table 2.

Notably, our study of implicit regularization suggests that the behavior of *nonconvex optimization* algorithms for statistical estimation needs to be examined in the context of *statistical models*, which induces an objective function as a finite sum. Our proof is accomplished via a leave-one-out perturbation argument, which is inherently tied to statistical models and leverages *homogeneity* across samples. Altogether, this allows us to localize benign landscapes for optimization and characterize finer dynamics not accounted for in generic gradient descent theory.

1.6 Notation

Before continuing, we introduce several notations used throughout the paper. First of all, boldfaced symbols are reserved for vectors and matrices. For any vector $\boldsymbol{v}$, we use $\|\boldsymbol{v}\|_2$ to denote its Euclidean norm. For any matrix $\boldsymbol{A}$, we use $\sigma_j(\boldsymbol{A})$ and $\lambda_j(\boldsymbol{A})$ to denote its jth largest singular value and eigenvalue, respectively. In addition, $\|\boldsymbol{A}\|$, $\|\boldsymbol{A}\|_{\mathrm{F}}$, $\|\boldsymbol{A}\|_{2,\infty}$, and $\|\boldsymbol{A}\|_\infty$ stand for the spectral norm (i.e. the largest singular value), the Frobenius norm, the ℓ_2/ℓ_∞ norm (i.e. the largest ℓ_2 norm of the rows), and the entrywise ℓ_∞ norm (the largest magnitude of all entries) of a matrix $\boldsymbol{A}$. Also, $\boldsymbol{A}^\top$, $\boldsymbol{A}^*$ and $\overline{\boldsymbol{A}}$ denote the transpose, the conjugate transpose, and the entrywise conjugate of $\boldsymbol{A}$, respectively. The notation $\mathcal{O}^{n\times r}$ represents the set of all $n \times r$ orthonormal matrices. The notation $[n]$ refers to the set $\{1, \cdots, n\}$. Throughout the paper, we use the terms "samples" and "measurements" interchangeably.

Additionally, the standard notation $f(n) = O(g(n))$ or $f(n) \lesssim g(n)$ means that there exists a constant $c > 0$ such that $|f(n)| \leq c|g(n)|$, $f(n) \gtrsim g(n)$ means that there exists a constant $c > 0$ such that $|f(n)| \geq c\,|g(n)|$, and $f(n) \asymp g(n)$ means that there exist constants $c_1, c_2 > 0$ such that $c_1|g(n)| \leq |f(n)| \leq c_2|g(n)|$.

2 Implicit regularization – a case study

To reveal reasons behind the effectiveness of vanilla gradient descent, we first examine existing theory of gradient descent and identify the geometric properties that enable linear convergence. We then develop an understanding as to why prior theory is conservative, and describe the phenomenon of implicit regularization that helps explain the effectiveness of vanilla GD. To facilitate discussion, we will use the problem of solving random quadratic systems (phase retrieval) and Wirtinger flow as a case study, but our diagnosis applies more generally, as will be seen in later sections.

2.1 Gradient descent theory revisited

In the convex optimization literature, there are two standard conditions about the objective function — strong convexity and smoothness — that allow for linear convergence of gradient descent.

Definition 1 (Strong convexity)**.** *A twice continuously differentiable function $f : \mathbb{R}^n \mapsto \mathbb{R}$ is said to be α-strongly convex if*

$$\nabla^2 f(\boldsymbol{x}) \succeq \alpha \boldsymbol{I}, \qquad \forall \boldsymbol{x} \in \mathbb{R}^n.$$

Definition 2 (Smoothness)**.** *A twice continuously differentiable function $f : \mathbb{R}^n \mapsto \mathbb{R}$ is said to be β-smooth if*

$$\left\|\nabla^2 f(\boldsymbol{x})\right\| \leq \beta, \qquad \forall \boldsymbol{x} \in \mathbb{R}^n.$$

It is well known that for an unconstrained optimization problem, if the objective function f is α-strongly convex and β-smooth, then vanilla gradient descent (4) enjoys ℓ_2 error contraction [B+15, Theorem 3.12], namely,

$$\left\|\boldsymbol{x}^{t+1} - \boldsymbol{x}^\natural\right\|_2 \leq \left(1 - \frac{2}{\beta/\alpha + 1}\right)\left\|\boldsymbol{x}^t - \boldsymbol{x}^\natural\right\|_2, \quad \text{and} \quad \left\|\boldsymbol{x}^t - \boldsymbol{x}^\natural\right\|_2 \leq \left(1 - \frac{2}{\beta/\alpha + 1}\right)^t \left\|\boldsymbol{x}^0 - \boldsymbol{x}^\natural\right\|_2, \quad t \geq 0, \tag{8}$$

as long as the step size is chosen as $\eta_t = 2/(\alpha + \beta)$. Here, $\boldsymbol{x}^\natural$ denotes the global minimum. This immediately reveals the iteration complexity for gradient descent: the number of iterations taken to attain ϵ-accuracy (in a relative sense) is bounded by

$$O\left(\frac{\beta}{\alpha}\log\frac{1}{\epsilon}\right).$$

In other words, the iteration complexity is dictated by and scales linearly with the condition number — the ratio β/α of smoothness to strong convexity parameters.

Moving beyond convex optimization, one can easily extend the above theory to *nonconvex* problems with *local* strong convexity and smoothness. More precisely, suppose the objective function f satisfies

$$\nabla^2 f(\boldsymbol{x}) \succeq \alpha \boldsymbol{I} \qquad \text{and} \qquad \left\|\nabla^2 f(\boldsymbol{x})\right\| \leq \beta$$

over a local ℓ_2 ball surrounding the global minimum $\boldsymbol{x}^\natural$:

$$\left\{\boldsymbol{x} \mid \|\boldsymbol{x} - \boldsymbol{x}^\natural\|_2 \leq \delta\|\boldsymbol{x}^\natural\|_2\right\}. \tag{9}$$

Then the contraction result (8) continues to hold, as long as the algorithm is seeded with an initial point that falls inside (9).

2.2 Local geometry for solving random quadratic systems

To invoke generic gradient descent theory, it is critical to characterize the local strong convexity and smoothness properties of the loss function. Take the problem of solving random quadratic systems (phase retrieval) as a case study. Consider the i.i.d. Gaussian design in which $\boldsymbol{a}_j \overset{\text{i.i.d.}}{\sim} \mathcal{N}(\boldsymbol{0}, \boldsymbol{I}_n)$, $1 \leq j \leq m$, and suppose without loss of generality that the underlying signal obeys $\|\boldsymbol{x}^\natural\|_2 = 1$. It is well known that $\boldsymbol{x}^\natural$ is the unique minimizer — up to global phase — of (2) under this statistical model, provided that the ratio m/n of equations to unknowns is sufficiently large. The Hessian of the loss function $f(\boldsymbol{x})$ is given by

$$\nabla^2 f(\boldsymbol{x}) = \frac{1}{m} \sum_{j=1}^{m} \left[3 \left(\boldsymbol{a}_j^\top \boldsymbol{x} \right)^2 - y_j \right] \boldsymbol{a}_j \boldsymbol{a}_j^\top . \tag{10}$$

- *Population-level analysis.* Consider the case with an infinite number of equations or samples, i.e. $m \to \infty$, where $\nabla^2 f(\boldsymbol{x})$ converges to its expectation. Simple calculation yields that

  $$\mathbb{E}\big[\nabla^2 f(\boldsymbol{x})\big] = 3\left(\|\boldsymbol{x}\|_2^2 \boldsymbol{I} + 2\boldsymbol{x}\boldsymbol{x}^\top\right) - \left(\boldsymbol{I} + 2\boldsymbol{x}^\natural \boldsymbol{x}^{\natural\top}\right).$$

  It it straightforward to verify that for any sufficiently small constant $\delta > 0$, one has the crude bound

  $$\boldsymbol{I} \preceq \mathbb{E}\big[\nabla^2 f(\boldsymbol{x})\big] \preceq 10\boldsymbol{I}, \qquad \forall \boldsymbol{x} : \big\|\boldsymbol{x} - \boldsymbol{x}^\natural\big\|_2 \leq \delta \big\|\boldsymbol{x}^\natural\big\|_2,$$

  meaning that f is 1-strongly convex and 10-smooth within a local ball around $\boldsymbol{x}^\natural$. As a consequence, when we have infinite samples and an initial guess with $\|\boldsymbol{x}^0 - \boldsymbol{x}^\natural\|_2 \leq \delta \big\|\boldsymbol{x}^\natural\big\|_2$, vanilla gradient descent with a constant step size converges to the global minimum within logarithmic iterations.

- *Finite-sample regime with $m \asymp n \log n$.* Now that f exhibits favorable landscape in the population level, one thus hopes that the fluctuation can be well-controlled so that the nice geometry carries over to the finite-sample regime. In the regime where $m \asymp n \log n$ (which is the regime considered in [CLS15]), the local strong convexity is still preserved, in the sense that

  $$\nabla^2 f(\boldsymbol{x}) \succeq \frac{1}{2}\boldsymbol{I}, \qquad \forall \boldsymbol{x} : \ \big\|\boldsymbol{x} - \boldsymbol{x}^\natural\big\|_2 \leq \delta \big\|\boldsymbol{x}^\natural\big\|_2$$

  occurs with high probability, provided that $\delta > 0$ is sufficiently small (see [Sol14, WWS15] and Lemma 1). The smoothness parameter, however, is not well-controlled. In fact, it can be as large as (up to logarithmic factors)[4]

  $$\big\|\nabla^2 f(\boldsymbol{x})\big\| \gtrsim n$$

  even when we restrict attention to the local ℓ_2 ball (9) with $\delta > 0$ being a fixed small constant. This means that the condition number β/α (defined in Section 2.1) may scale as $O(n)$, leading to the step size recommendation

  $$\eta_t \asymp 1/n$$

  and, as a consequence, a high iteration complexity $O(n \log \frac{1}{\epsilon})$. This underpins the analysis in [CLS15].

In summary, the geometric properties of the loss function — even in the local ℓ_2 ball centering around the global minimum — is not as favorable as one anticipates, in particular in view of its population counterpart. A direct application of generic gradient descent theory leads to an overly conservative step size and a pessimistic convergence rate, unless the number of samples is enormously larger than the number of unknowns.

Remark 2. Notably, due to Gaussian designs, the phase retrieval problem enjoys more favorable geometry compared to other nonconvex problems. In matrix completion and blind deconvolution, the Hessian matrices are rank-deficient even at the population level. In such cases, the above discussions need to be adjusted, e.g. strong convexity is only possible when we restrict attention to certain directions.

[4] To demonstrate this, take $\boldsymbol{x} = \boldsymbol{x}^\natural + \frac{\boldsymbol{a}_1}{\|\boldsymbol{a}_1\|_2}\delta$ in (10), one can easily verify that, with high probability, $\big\|\nabla^2 f(\boldsymbol{x})\big\| \geq \frac{|3(\boldsymbol{a}_1^\top \boldsymbol{x})^2 - y_1|}{m} \big\|\boldsymbol{a}_1 \boldsymbol{a}_1^\top\big\| - O(1) \gtrsim \frac{\delta^2 n^2}{m} \asymp \delta^2 \frac{n}{\log n}$.

2.3 Which region enjoys nicer geometry? Incoherence!

Interestingly, our theory identifies a local region surrounding $\boldsymbol{x}^\natural$ with a large diameter that enjoys much better behaved geometry. This region does not mimic an ℓ_2 ball, but rather, the intersection of an ℓ_2 ball and a polytope. We term it the *region of incoherence and contraction* (RIC). For phase retrieval, the RIC includes all points $\boldsymbol{x} \in \mathbb{R}^n$ obeying

$$\left\|\boldsymbol{x} - \boldsymbol{x}^\natural\right\|_2 \le \delta \left\|\boldsymbol{x}^\natural\right\|_2 \qquad \text{and} \tag{11a}$$

$$\max_{1\le j\le m} \left|\boldsymbol{a}_j^\top \left(\boldsymbol{x} - \boldsymbol{x}^\natural\right)\right| \lesssim \sqrt{\log n}\left\|\boldsymbol{x}^\natural\right\|_2, \tag{11b}$$

where $\delta > 0$ is some numerical constant. As will be formalized in Lemma 1, with high probability the Hessian matrix satisfies

$$\frac{1}{2}\boldsymbol{I} \preceq \nabla^2 f(\boldsymbol{x}) \preceq O(\log n)\cdot \boldsymbol{I}$$

simultaneously for $\boldsymbol{x}$ in the RIC. In words, the Hessian matrix is nearly well-conditioned (with the condition number bounded by $O(\log n)$), as long as (i) the iterate is not very far from the global minimizer (cf. (11a)), and (ii) the iterate remains incoherent[5] with respect to the sensing vectors (cf. (11b)). Another way to interpret the incoherence condition (11b) is that the empirical risk needs to be well-controlled uniformly across all samples. See Figure 2(a) for an illustration of the above region.

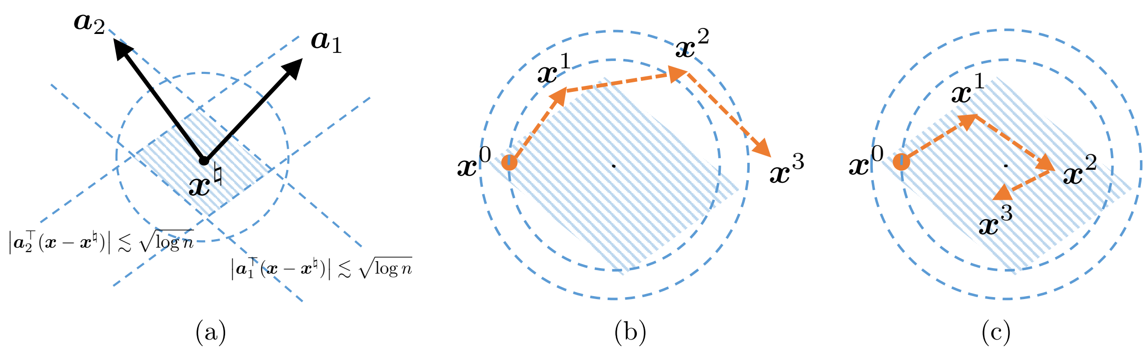

Figure 2: (a) The shaded region is an example of the incoherence region, which satisfies $\left|\boldsymbol{a}_j^\top(\boldsymbol{x}-\boldsymbol{x}^\natural)\right| \lesssim \sqrt{\log n}$ for all points $\boldsymbol{x}$ in the region. (b) When $\boldsymbol{x}^0$ resides in the desired region, we know that $\boldsymbol{x}^1$ remains within the ℓ_2 ball but might fall out of the incoherence region (the shaded region). Once $\boldsymbol{x}^1$ leaves the incoherence region, we lose control and may overshoot. (c) Our theory reveals that with high probability, all iterates will stay within the incoherence region, enabling fast convergence.

The following observation is thus immediate: one can safely adopt a far more aggressive step size (as large as $\eta_t = O(1/\log n)$) to achieve acceleration, as long as iterates stay within the RIC. This, however, fails to be guaranteed by generic gradient descent theory. To be more precise, if the current iterate $\boldsymbol{x}^t$ falls within the desired region, then in view of (8), we can ensure ℓ_2 error contraction after one iteration, namely,

$$\|\boldsymbol{x}^{t+1} - \boldsymbol{x}^\natural\|_2 \le \|\boldsymbol{x}^t - \boldsymbol{x}^\natural\|_2$$

and hence $\boldsymbol{x}^{t+1}$ stays within the ℓ_2 ball and satisfies (11a). However, it is not immediately obvious that $\boldsymbol{x}^{t+1}$ would still stay incoherent with the sensing vectors and satisfy (11b). If $\boldsymbol{x}^{t+1}$ leaves the RIC, we lose control of the geometry of the loss function, and the algorithm has to slow down in order to avoid overshooting. See Figure 2(b) for a visual illustration. In fact, in almost all regularized gradient descent algorithms mentioned in Section 1.2, the regularization procedures are designed to enforce such incoherence constraints.

[5]If $\boldsymbol{x}$ is aligned with (and hence very coherent to) one vector $\boldsymbol{a}_j$, then with high probability one has $\left|\boldsymbol{a}_j^\top(\boldsymbol{x}-\boldsymbol{x}^\natural)\right| \gtrsim |\boldsymbol{a}_j^\top\boldsymbol{x}| \asymp \sqrt{n}\|\boldsymbol{x}\|_2$, which is significantly larger than $\sqrt{\log n}\|\boldsymbol{x}\|_2$.

2.4 Implicit regularization

However, is regularization really necessary for the iterates to stay within the RIC? To answer this question, we plot in Figure 3(a) (resp. Figure 3(b)) the incoherence measure $\frac{\max_j \left|\boldsymbol{a}_j^\top \boldsymbol{x}^t\right|}{\sqrt{\log n}\|\boldsymbol{x}^\natural\|_2}$ (resp. $\frac{\max_j \left|\boldsymbol{a}_j^\top (\boldsymbol{x}^t - \boldsymbol{x}^\natural)\right|}{\sqrt{\log n}\|\boldsymbol{x}^\natural\|_2}$) vs. the iteration count in a typical Monte Carlo trial, generated in the same way as for Figure 1(a). Interestingly, the incoherence measure remains bounded by 2 for all iterations $t > 1$. This important observation suggests that one may adopt a substantially more aggressive step size throughout the whole algorithm.

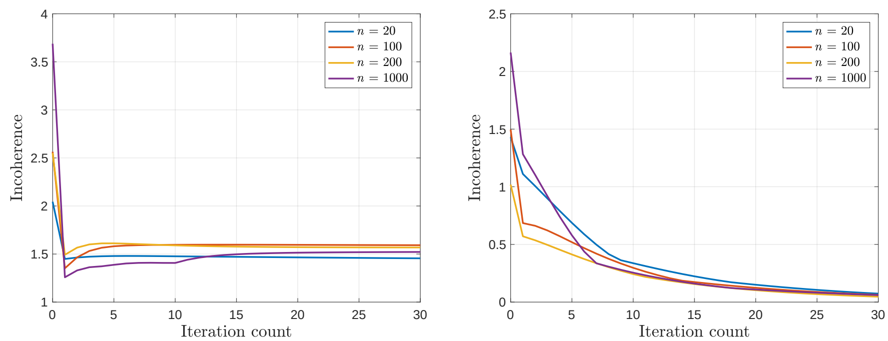

(a) (b)

Figure 3: The incoherence measure $\frac{\max_{1\leq j\leq m} \left|\boldsymbol{a}_j^\top \boldsymbol{x}^t\right|}{\sqrt{\log n}\|\boldsymbol{x}^\natural\|_2}$ (in (a)) and $\frac{\max_{1\leq j\leq m} \left|\boldsymbol{a}_j^\top (\boldsymbol{x}^t - \boldsymbol{x}^\natural)\right|}{\sqrt{\log n}\|\boldsymbol{x}^\natural\|_2}$ (in (b)) of the gradient iterates vs. iteration count for the phase retrieval problem. The results are shown for $n \in \{20, 100, 200, 1000\}$ and $m = 10n$, with the step size taken to be $\eta_t = 0.1$. The problem instances are generated in the same way as in Figure 1(a).

The main objective of this paper is thus to provide a theoretical validation of the above empirical observation. As we will demonstrate shortly, with high probability all iterates (as well as the spectral initialization) are provably constrained within the RIC throughout the execution of the algorithm, implying fast convergence of vanilla gradient descent (cf. Figure 2(c)). The fact that the iterates stay incoherent with the measurement mechanism automatically, without explicit enforcement, is termed "implicit regularization".

2.5 A glimpse of the analysis: a leave-one-out trick

In order to rigorously establish (11b) for all iterates, the current paper develops a powerful mechanism based on a leave-one-out perturbation argument, a trick rooted and widely used in probability and random matrix theory. Note that the iterate $\boldsymbol{x}^t$ is statistically dependent of the design vectors $\boldsymbol{a}_j$'s. Under such circumstances, one often resorts to generic bounds like the Cauchy-Schwarz inequality, which would not yield a desirable estimate. To address this issue, we introduce a sequence of auxiliary iterates $\{\boldsymbol{x}^{t,(l)}\}$ for each $1 \leq l \leq m$ (for analytical purposes only), obtained by running vanilla gradient descent using all but the lth sample. As one can expect, such auxiliary trajectories serve as extremely good surrogates of $\{\boldsymbol{x}^t\}$ in the sense that

$$\boldsymbol{x}^t \approx \boldsymbol{x}^{t,(l)}, \qquad 1 \leq l \leq m, \quad t \geq 0, \tag{12}$$

since their constructions only differ by a single sample. Most importantly, since $\boldsymbol{x}^{t,(l)}$ is independent from the lth design vector, it is much easier to control its incoherence w.r.t. $\boldsymbol{a}_l$ to the desired level:

$$\left|\boldsymbol{a}_l^\top \left(\boldsymbol{x}^{t,(l)} - \boldsymbol{x}^\natural\right)\right| \lesssim \sqrt{\log n}\, \left\|\boldsymbol{x}^\natural\right\|_2. \tag{13}$$

Combining (12) and (13) then leads to (11b). See Figure 4 for a graphical illustration of this argument. Notably, this technique is very general and applicable to many other problems. We invite the readers to Section 5 for more details.

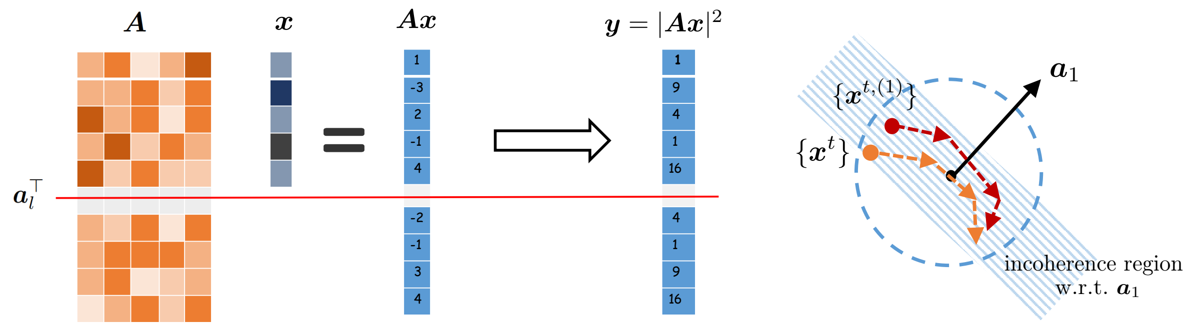

(a) (b)

Figure 4: Illustration of the leave-one-out sequence. (a) The sequence $\{\boldsymbol{x}^{t,(l)}\}$ is constructed without using the lth sample. (b) Since the auxiliary sequence $\{\boldsymbol{x}^{t,(1)}\}$ is constructed without using $\boldsymbol{a}_1$, the leave-one-out iterates stay within the incoherence region w.r.t. $\boldsymbol{a}_1$ with high probability. Meanwhile, $\{\boldsymbol{x}^t\}$ and $\{\boldsymbol{x}^{t,(1)}\}$ are expected to remain close as their construction differ only in a single sample.

3 Main results

This section formalizes the implicit regularization phenomenon underlying unregularized gradient descent, and presents its consequences (namely, near-optimal statistical and computational guarantees) for phase retrieval, matrix completion, and blind deconvolution. Note that the distance metric may vary from problem to problem.

3.1 Phase retrieval

Suppose the m quadratic equations

$$y_j = \left(\boldsymbol{a}_j^\top \boldsymbol{x}^\natural\right)^2, \qquad j = 1, 2, \ldots, m \tag{14}$$

are collected using random design vectors, namely, $\boldsymbol{a}_j \overset{\text{i.i.d.}}{\sim} \mathcal{N}(\boldsymbol{0}, \boldsymbol{I}_n)$, and the nonconvex problem to solve is

$$\text{minimize}_{\boldsymbol{x}\in\mathbb{R}^n} \quad f(\boldsymbol{x}) := \frac{1}{4m}\sum_{j=1}^{m}\left[\left(\boldsymbol{a}_j^\top \boldsymbol{x}\right)^2 - y_j\right]^2. \tag{15}$$

The Wirtinger flow (WF) algorithm, first introduced in [CLS15], is a combination of spectral initialization and vanilla gradient descent; see Algorithm 1.

Algorithm 1 Wirtinger flow for phase retrieval

Input: $\{\boldsymbol{a}_j\}_{1\le j\le m}$ and $\{y_j\}_{1\le j\le m}$.
Spectral initialization: Let $\lambda_1(\boldsymbol{Y})$ and $\tilde{\boldsymbol{x}}^0$ be the leading eigenvalue and eigenvector of

$$\boldsymbol{Y} = \frac{1}{m}\sum_{j=1}^{m} y_j \boldsymbol{a}_j \boldsymbol{a}_j^\top, \tag{16}$$

respectively, and set $\boldsymbol{x}^0 = \sqrt{\lambda_1(\boldsymbol{Y})/3}\,\tilde{\boldsymbol{x}}^0$.
Gradient updates: **for** $t = 0, 1, 2, \ldots, T-1$ **do**

$$\boldsymbol{x}^{t+1} = \boldsymbol{x}^t - \eta_t \nabla f\left(\boldsymbol{x}^t\right). \tag{17}$$

Recognizing that the global phase/sign is unrecoverable from quadratic measurements, we introduce the ℓ_2 distance modulo the global phase as follows

$$\text{dist}(\boldsymbol{x}, \boldsymbol{x}^\natural) := \min\left\{\|\boldsymbol{x} - \boldsymbol{x}^\natural\|_2, \|\boldsymbol{x} + \boldsymbol{x}^\natural\|_2\right\}. \tag{18}$$

Our finding is summarized in the following theorem.

Theorem 1. *Let $\boldsymbol{x}^\natural \in \mathbb{R}^n$ be a fixed vector. Suppose $\boldsymbol{a}_j \overset{\text{i.i.d.}}{\sim} \mathcal{N}(\boldsymbol{0}, \boldsymbol{I}_n)$ for each $1 \le j \le m$ and $m \ge c_0 n \log n$ for some sufficiently large constant $c_0 > 0$. Assume the step size obeys $\eta_t \equiv \eta = \frac{c_1}{\log n}$ for any sufficiently small constant $c_1 > 0$. Then there exist some absolute constants $0 < \varepsilon < 1$ and $c_2 > 0$ such that with probability at least $1 - O(mn^{-5})$, the Wirtinger flow iterates (Algorithm 1) satisfy that for all $t \ge 0$,*

$$\operatorname{dist}(\boldsymbol{x}^t, \boldsymbol{x}^\natural) \le \varepsilon (1 - \eta/2)^t \|\boldsymbol{x}^\natural\|_2, \tag{19a}$$

$$\max_{1 \le j \le m} \left| \boldsymbol{a}_j^\top \left(\boldsymbol{x}^t - \boldsymbol{x}^\natural \right) \right| \le c_2 \sqrt{\log n} \|\boldsymbol{x}^\natural\|_2. \tag{19b}$$

Theorem 1 reveals a few intriguing properties of WF.

- **Implicit regularization:** Theorem 1 asserts that the incoherence properties are satisfied throughout the execution of the algorithm (see (19b)), which formally justifies the implicit regularization feature we hypothesized.
- **Near-constant step size:** Theorem 1 establishes near-linear convergence of WF with a substantially more aggressive step size $\eta \asymp 1/\log n$. Compared with the choice $\eta \lesssim 1/n$ admissible in [CLS15, Theorem 3.3], Theorem 1 allows WF to attain ϵ-accuracy within $O(\log n \log(1/\epsilon))$ iterations. The resulting computational complexity of WF is
$$O\left(mn \log n \log \frac{1}{\epsilon} \right),$$
which significantly improves upon the result $O(mn^2 \log \frac{1}{\epsilon})$ derived in [CLS15].
- **Incoherence of spectral initialization:** We have also demonstrated in Theorem 1 that the initial guess falls within the RIC and are hencee nearly orthogonal to all design vectors. This provides a finer characterization of spectral initialization, in comparison to the prior theory that focuses primarily on the ℓ_2 accuracy [NJS13, CLS15]. We expect our leave-one-out analysis to accommodate other variants of spectral initialization studied in the literature [CC17, CLM+16, WGE17, LL17, MM17].

3.2 Low-rank matrix completion

Let $\boldsymbol{M}^\natural \in \mathbb{R}^{n \times n}$ be a positive semidefinite matrix with rank r whose eigendecomposition is given by $\boldsymbol{M}^\natural = \boldsymbol{U}^\natural \boldsymbol{\Sigma}^\natural \boldsymbol{U}^{\natural\top}$, where $\boldsymbol{U}^\natural \in \mathbb{R}^{n \times r}$ consists of orthonormal columns, and $\boldsymbol{\Sigma}^\natural$ is an $r \times r$ diagonal matrix with eigenvalues in descending order, i.e. $\sigma_{\max} = \sigma_1 \ge \cdots \ge \sigma_r = \sigma_{\min} > 0$.[6] Throughout this paper, we assume the condition number $\kappa := \sigma_{\max}/\sigma_{\min}$ is bounded by a fixed constant. Denoting $\boldsymbol{X}^\natural = \boldsymbol{U}^\natural (\boldsymbol{\Sigma}^\natural)^{1/2}$ allows us to factorize $\boldsymbol{M}^\natural$ as

$$\boldsymbol{M}^\natural = \boldsymbol{X}^\natural \boldsymbol{X}^{\natural\top}. \tag{20}$$

Consider a random sampling model such that each entry of $\boldsymbol{M}^\natural$ is observed independently with probability $0 < p \le 1$, i.e. for $1 \le j \le k \le n$,

$$Y_{j,k} \overset{\text{ind.}}{=} \begin{cases} M^\natural_{j,k} + E_{j,k} & \text{with probability } p, \\ 0, & \text{else,} \end{cases} \tag{21}$$

where the entries of $\boldsymbol{E} = [E_{j,k}]_{1 \le j \le k \le n}$ are independent sub-Gaussian noise with sub-Gaussian norm σ (see [Ver12, Definition 5.7]). We denote by Ω the set of locations being sampled, and $\mathcal{P}_\Omega(\boldsymbol{Y})$ denotes the projection of $\boldsymbol{Y}$ onto the set of matrices supported in Ω.

To fix ideas, we consider the following nonconvex optimization problem

$$\text{minimize}_{\boldsymbol{X} \in \mathbb{R}^{n \times r}} \quad f(\boldsymbol{X}) := \frac{1}{4p} \sum_{(j,k) \in \Omega} \left(\boldsymbol{e}_j^\top \boldsymbol{X} \boldsymbol{X}^\top \boldsymbol{e}_k - Y_{j,k} \right)^2. \tag{22}$$

The vanilla gradient descent algorithm (with spectral initialization) is summarized in Algorithm 2.

[6] Here, we assume that $\boldsymbol{M}^\natural$ takes this form to simplify presentation, but note that our analysis easily extends to asymmetric low-rank matrices.

Algorithm 2 Vanilla gradient descent for matrix completion (with spectral initialization)

Input: $\boldsymbol{Y} = [Y_{j,k}]_{1\leq j,k\leq n}$, r, p.

Spectral initialization: Let $\boldsymbol{U}^0\boldsymbol{\Sigma}^0\boldsymbol{U}^{0\top}$ be the rank-r eigendecomposition of

$$\boldsymbol{M}^0 := \frac{1}{p}\mathcal{P}_\Omega(\boldsymbol{Y}) = \frac{1}{p}\mathcal{P}_\Omega\left(\boldsymbol{M}^\natural + \boldsymbol{E}\right),$$

and set $\boldsymbol{X}^0 = \boldsymbol{U}^0\left(\boldsymbol{\Sigma}^0\right)^{1/2}$.

Gradient updates: **for** $t = 0, 1, 2, \ldots, T-1$ **do**

$$\boldsymbol{X}^{t+1} = \boldsymbol{X}^t - \eta_t \nabla f\left(\boldsymbol{X}^t\right). \tag{23}$$

Before proceeding to the main theorem, we first introduce a standard incoherence parameter required for matrix completion [CR09].

Definition 3 (Incoherence for matrix completion). *A rank-r matrix $\boldsymbol{M}^\natural$ with eigendecomposition $\boldsymbol{M}^\natural = \boldsymbol{U}^\natural\boldsymbol{\Sigma}^\natural\boldsymbol{U}^{\natural\top}$ is said to be μ-incoherent if*

$$\left\|\boldsymbol{U}^\natural\right\|_{2,\infty} \leq \sqrt{\frac{\mu}{n}}\left\|\boldsymbol{U}^\natural\right\|_{\mathrm{F}} = \sqrt{\frac{\mu r}{n}}. \tag{24}$$

In addition, recognizing that $\boldsymbol{X}^\natural$ is identifiable only up to orthonormal transformation, we define the optimal rotation from the tth iterate $\boldsymbol{X}^t$ to $\boldsymbol{X}^\natural$ as

$$\hat{\boldsymbol{H}}^t := \underset{\boldsymbol{R}\in\mathcal{O}^{r\times r}}{\operatorname{argmin}}\left\|\boldsymbol{X}^t\boldsymbol{R} - \boldsymbol{X}^\natural\right\|_{\mathrm{F}}, \tag{25}$$

where $\mathcal{O}^{r\times r}$ is the set of $r\times r$ orthonormal matrices. With these definitions in place, we have the following theorem.

Theorem 2. *Let $\boldsymbol{M}^\natural$ be μ-incoherent, and its condition number κ is a fixed constant. Suppose the sample size satisfies $n^2p \geq C\mu^3r^3n\log^3 n$ for some sufficiently large constant $C > 0$, and the noise satisfies*

$$\sigma\sqrt{\frac{n}{p}} \lesssim \frac{\sigma_{\min}}{\sqrt{\mu r\log^3 n}}. \tag{26}$$

With probability at least $1 - O\left(n^{-3}\right)$, the iterates of Algorithm 2 satisfy

$$\left\|\boldsymbol{X}^t\hat{\boldsymbol{H}}^t - \boldsymbol{X}^\natural\right\|_{\mathrm{F}} \leq \left(C_4\rho^t\mu r\frac{1}{\sqrt{np}} + C_1\frac{\sigma}{\sigma_{\min}}\sqrt{\frac{n}{p}}\right)\left\|\boldsymbol{X}^\natural\right\|_{\mathrm{F}}, \tag{27a}$$

$$\left\|\boldsymbol{X}^t\hat{\boldsymbol{H}}^t - \boldsymbol{X}^\natural\right\|_{2,\infty} \leq \left(C_5\rho^t\mu r\sqrt{\frac{\log n}{np}} + C_8\frac{\sigma}{\sigma_{\min}}\sqrt{\frac{n\log n}{p}}\right)\left\|\boldsymbol{X}^\natural\right\|_{2,\infty}, \tag{27b}$$

$$\left\|\boldsymbol{X}^t\hat{\boldsymbol{H}}^t - \boldsymbol{X}^\natural\right\| \leq \left(C_9\rho^t\mu r\frac{1}{\sqrt{np}} + C_{10}\frac{\sigma}{\sigma_{\min}}\sqrt{\frac{n}{p}}\right)\left\|\boldsymbol{X}^\natural\right\| \tag{27c}$$

for all $0 \leq t \leq T = O(n^5)$, where C_1, C_4, C_5, C_8, C_9 and C_{10} are some absolute positive constants and $\rho \geq 1 - \frac{\sigma_{\min}}{5}\eta$, provided that $0 < \eta_t \equiv \eta \leq \frac{2}{25\kappa\sigma_{\max}}$.

Theorem 2 provides the first theoretical guarantee of unregularized gradient descent for matrix completion, demonstrating near-optimal statistical accuracy and computational complexity.

- **Implicit regularization:** In Theorem 2, we bound the ℓ_2/ℓ_∞ error of the iterates in a uniform manner via (27b). Note that $\left\|\boldsymbol{X} - \boldsymbol{X}^\natural\right\|_{2,\infty} = \max_{1\leq j\leq n}\left\|\boldsymbol{e}_j^\top\left(\boldsymbol{X} - \boldsymbol{X}^\natural\right)\right\|_2$, which implies the iterates remain incoherent with the sensing vectors throughout and have small incoherence parameters (cf. (24)). This means an explicit regularization to promote incoherence is unnecessary.

- **Constant step size:** Theorem 2 guarantees the iterates of vanilla gradient descent converges linearly at a constant step size $\eta \asymp 1$. Remarkably, the convergence occurs with respect to three different unitarily invariant norms: the Frobenius norm $\|\cdot\|_{\mathrm{F}}$, the ℓ_2/ℓ_∞ norm $\|\cdot\|_{2,\infty}$, and the spectral norm $\|\cdot\|$. As far as we know, the latter two are established for the first time. Notably, such a constant step size even improves upon the requirement of regularized gradient descent; see Table 1.

- **Near-optimal sample complexity:** When the rank $r = O(1)$, vanilla gradient descent succeeds under a near-optimal sample complexity $n^2 p \gtrsim n \mathrm{poly} \log n$, which is statistically optimal up to some logarithmic factor.

- **Near-minimal Euclidean error:** From (27a), as t increases the Euclidean error of vanilla GD converges to
$$\left\|\boldsymbol{X}^t \hat{\boldsymbol{H}}^t - \boldsymbol{X}^\natural\right\|_{\mathrm{F}} \lesssim \frac{\sigma}{\sigma_{\min}}\sqrt{\frac{n}{p}}\left\|\boldsymbol{X}^\natural\right\|_{\mathrm{F}} \tag{28}$$
which coincides with the theoretical guarantee in [CW15, Corollary 1] and matches the minimax lower bounds in [NW12, KLT11].

- **Near-optimal entrywise error:** The ℓ_2/ℓ_∞ error bound (27b) immediately yields entrywise control of the empirical risk. Specifically, as soon as t is sufficiently large (so that the first term in (27b) is negligible), we have
$$\begin{aligned}\left\|\boldsymbol{X}^t \boldsymbol{X}^{t\top} - \boldsymbol{M}^\natural\right\|_\infty &\leq \left\|\boldsymbol{X}^t \hat{\boldsymbol{H}}^t \left(\boldsymbol{X}^t \hat{\boldsymbol{H}}^t - \boldsymbol{X}^\natural\right)^\top\right\|_\infty + \left\|\left(\boldsymbol{X}^t \hat{\boldsymbol{H}}^t - \boldsymbol{X}^\natural\right)\boldsymbol{X}^{\natural\top}\right\|_\infty \\ &\leq \left\|\boldsymbol{X}^t \hat{\boldsymbol{H}}^t\ \right\|_{2,\infty}\left\|\boldsymbol{X}^t \hat{\boldsymbol{H}}^t - \boldsymbol{X}^\natural\right\|_{2,\infty} + \left\|\boldsymbol{X}^t \hat{\boldsymbol{H}}^t - \boldsymbol{X}^\natural\right\|_{2,\infty}\left\|\boldsymbol{X}^\natural\right\|_{2,\infty} \\ &\lesssim \frac{\sigma}{\sigma_{\min}}\sqrt{\frac{n\log n}{p}}\left\|\boldsymbol{M}^\natural\right\|_\infty,\end{aligned}$$
where the last line follows from (27b) as well as the facts that $\left\|\boldsymbol{X}^t \hat{\boldsymbol{H}}^t - \boldsymbol{X}^\natural\right\|_{2,\infty} \leq \left\|\boldsymbol{X}^\natural\right\|_{2,\infty}$ and $\left\|\boldsymbol{M}^\natural\right\|_\infty = \left\|\boldsymbol{X}^\natural\right\|_{2,\infty}^2$. Compared with the Euclidean loss (28), this implies that when $r = O(1)$, the entrywise error of $\boldsymbol{X}^t \boldsymbol{X}^{t\top}$ is uniformly spread out across all entries. As far as we know, this is the first result that reveals near-optimal entrywise error control for noisy matrix completion using nonconvex optimization, without resorting to sample splitting.

Remark 3. Theorem 2 remains valid if the total number T of iterations obeys $T = n^{O(1)}$. In the noiseless case where $\sigma = 0$, the theory allows $T \to \infty$.

Finally, we report the empirical statistical accuracy of vanilla GD in the presence of noise. Figure 5 displays the squared relative error of vanilla GD as a function of the signal-to-noise ratio (SNR), where the SNR is defined to be
$$\mathsf{SNR} := \frac{\sum_{(j,k)\in\Omega}\left(M_{j,k}^\natural\right)^2}{\sum_{(j,k)\in\Omega}\mathsf{Var}\left(E_{j,k}\right)} \approx \frac{\|\boldsymbol{M}^\natural\|_{\mathrm{F}}^2}{n^2\sigma^2}, \tag{29}$$
and the relative error is measured in terms of the square of the metrics as in (27) as well as the squared entrywise prediction error. Both the relative error and the SNR are shown on a dB scale (i.e. $10\log_{10}(\mathrm{SNR})$ and $10\log_{10}(\text{squared relative error})$ are plotted). As one can see from the plot, the squared relative error scales inversely proportional to the SNR, which is consistent with our theory.[7]

3.3 Blind deconvolution

Suppose we have collected m bilinear measurements
$$y_j = \boldsymbol{b}_j^* \boldsymbol{h}^\natural \boldsymbol{x}^{\natural *} \boldsymbol{a}_j, \qquad 1 \leq j \leq m, \tag{30}$$

[7]Note that when $\boldsymbol{M}^\natural$ is well-conditioned and when $r = O(1)$, one can easily check that $\mathsf{SNR} \approx \frac{\|\boldsymbol{M}^\natural\|_{\mathrm{F}}^2}{n^2\sigma^2} \asymp \frac{\sigma_{\min}^2}{n^2\sigma^2}$, and our theory says that the squared relative error bound is proportional to $\sigma^2/\sigma_{\min}^2$.

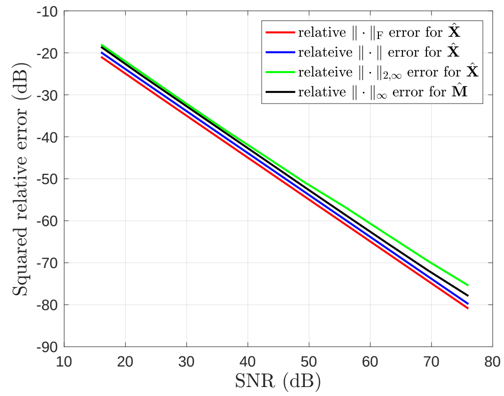

Figure 5: Squared relative error of the estimate $\hat{\boldsymbol{X}}$ (measured by $\|\cdot\|_{\mathrm{F}}, \|\cdot\|, \|\cdot\|_{2,\infty}$ modulo global transformation) and $\hat{\boldsymbol{M}} = \hat{\boldsymbol{X}}\hat{\boldsymbol{X}}^\top$ (measured by the relative entrywise ℓ_∞ norm) vs. SNR for noisy matrix completion, where $n = 500$, $r = 10$, $p = 0.1$, and $\eta_t = 0.2$.

where $\boldsymbol{a}_j$ follows a complex Gaussian distribution, i.e. $\boldsymbol{a}_j \overset{\text{i.i.d.}}{\sim} \mathcal{N}\left(\boldsymbol{0}, \frac{1}{2}\boldsymbol{I}_N\right) + i\mathcal{N}\left(\boldsymbol{0}, \frac{1}{2}\boldsymbol{I}_N\right)$, and $\boldsymbol{B} := [\boldsymbol{b}_1, \cdots, \boldsymbol{b}_m]^* \in \mathbb{C}^{m\times K}$ is formed by the first K columns of a unitary discrete Fourier transform (DFT) matrix $\boldsymbol{F} \in \mathbb{C}^{m\times m}$ obeying $\boldsymbol{F}\boldsymbol{F}^* = \boldsymbol{I}_m$. This setup models blind deconvolution, where the two signals under convolution belong to known low-dimensional subspaces of dimension K [ARR14][8]. In particular, the partial DFT matrix $\boldsymbol{B}$ plays an important role in blind deblurring for imaging applications. In this subsection, we consider solving the following nonconvex optimization problem

$$\text{minimize}_{\boldsymbol{h},\boldsymbol{x}\in\mathbb{C}^K} \quad f(\boldsymbol{h},\boldsymbol{x}) = \sum_{j=1}^m \left|\boldsymbol{b}_j^*\boldsymbol{h}\boldsymbol{x}^*\boldsymbol{a}_j - y_j\right|^2. \tag{31}$$

The (Wirtinger) gradient descent algorithm (with spectral initialization) is summarized in Algorithm 3; here, $\nabla_{\boldsymbol{h}} f(\boldsymbol{h},\boldsymbol{x})$ and $\nabla_{\boldsymbol{x}} f(\boldsymbol{h},\boldsymbol{x})$ stand for the Wirtinger gradient and are given in (75) and (76), respectively; see [CLS15, Section 6] for a brief introduction of Wirtinger calculus.

It is self-evident that $\boldsymbol{h}^\natural$ and $\boldsymbol{x}^\natural$ are not identifiable up to global scaling, that is, for any nonzero $\alpha \in \mathbb{C}$,

$$\boldsymbol{h}^\natural\boldsymbol{x}^{\natural *} = \frac{1}{\overline{\alpha}}\boldsymbol{h}^\natural\left(\alpha\boldsymbol{x}^\natural\right)^*.$$

In light of this, we will measure the distance between $\boldsymbol{z} := (\boldsymbol{h}^*, \boldsymbol{x}^*)^*$ and $\boldsymbol{z}^\natural := \left(\boldsymbol{h}^{\natural *}, \boldsymbol{x}^{\natural *}\right)^*$ via the following metric

$$\operatorname{dist}\left(\boldsymbol{z}, \boldsymbol{z}^\natural\right) := \min_{\alpha\in\mathbb{C}} \sqrt{\left\|\frac{1}{\overline{\alpha}}\boldsymbol{h} - \boldsymbol{h}^\natural\right\|_2^2 + \left\|\alpha\boldsymbol{x} - \boldsymbol{x}^\natural\right\|_2^2}. \tag{32}$$

Here and throughout, we abuse the notation $\operatorname{dist}(\cdot,\cdot)$ whenever it is clear from context.

Before proceeding, we need to introduce the incoherence parameter [ARR14, LLSW16], which is crucial for the blind deconvolution problem.

Definition 4 (incoherence for blind deconvolution)**.** *Let the incoherence parameter μ be the smallest number such that*

$$\max_{1\le j\le m} \left|\boldsymbol{b}_j^*\boldsymbol{h}^\natural\right| \le \frac{\mu}{\sqrt{m}}\left\|\boldsymbol{h}^\natural\right\|_2 = \frac{\mu}{\sqrt{m}}. \tag{34}$$

Theorem 3. *Suppose the number of measurements obeys $m \ge C\mu^2 K \log^8 m$ for some sufficiently large constant $C > 0$, and suppose the step size $\eta > 0$ is taken to be some sufficiently small constant. Then there*

[8]For simplicity, we have set the dimension of the two subspaces equal, and it is straightforward to extend our results to the case of unequal subspace dimensions.

Algorithm 3 Vanilla gradient descent for blind deconvolution (with spectral initialization)

Input: $\{\boldsymbol{a}_j\}_{1\leq j\leq m}$, $\{\boldsymbol{b}_j\}_{1\leq j\leq m}$ and $\{y_j\}_{1\leq j\leq m}$.

Spectral initialization: Let $\sigma_1(\boldsymbol{M})$, $\check{\boldsymbol{h}}^0$ and $\check{\boldsymbol{x}}^0$ be the leading singular value, left and right singular vectors of

$$\boldsymbol{M} := \sum_{j=1}^{m} y_j \boldsymbol{b}_j \boldsymbol{a}_j^*$$

respectively. Set $\boldsymbol{h}^0 = \sqrt{\sigma_1(\boldsymbol{M})}\,\check{\boldsymbol{h}}^0$ and $\boldsymbol{x}^0 = \sqrt{\sigma_1(\boldsymbol{M})}\,\check{\boldsymbol{x}}^0$.

Gradient updates: **for** $t = 0, 1, 2, \dots, T-1$ **do**

$$\begin{bmatrix} \boldsymbol{h}^{t+1} \\ \boldsymbol{x}^{t+1} \end{bmatrix} = \begin{bmatrix} \boldsymbol{h}^{t} \\ \boldsymbol{x}^{t} \end{bmatrix} - \eta \begin{bmatrix} \frac{1}{\|\boldsymbol{x}^t\|^2} \nabla_{\boldsymbol{h}} f\big(\boldsymbol{h}^t, \boldsymbol{x}^t\big) \\ \frac{1}{\|\boldsymbol{h}^t\|^2} \nabla_{\boldsymbol{x}} f\big(\boldsymbol{h}^t, \boldsymbol{x}^t\big) \end{bmatrix}. \tag{33}$$

exist constants $c_1, c_2, C_1, C_3, C_4 > 0$ *such that with probability exceeding* $1 - c_1 m^{-5} - c_1 m e^{-c_2 K}$*, the iterates in Algorithm 3 satisfy*

$$\mathrm{dist}\left(\boldsymbol{z}^t, \boldsymbol{z}^\natural\right) \leq C_1 \left(1 - \frac{\eta}{16}\right)^t \frac{1}{\log^2 m}, \tag{35a}$$

$$\max_{1\leq l\leq m} \left|\boldsymbol{a}_j^*\left(\alpha^t \boldsymbol{x}^t - \boldsymbol{x}^\natural\right)\right| \leq C_3 \frac{1}{\log^{1.5} m}, \tag{35b}$$

$$\max_{1\leq l\leq m} \left|\boldsymbol{b}_l^* \frac{1}{\overline{\alpha^t}} \boldsymbol{h}^t\right| \leq C_4 \frac{\mu}{\sqrt{m}} \log^2 m \tag{35c}$$

for all $t \geq 0$*. Here, we denote*

$$\alpha^t := \arg\min_{\alpha\in\mathbb{C}} \left\|\frac{1}{\overline{\alpha}}\boldsymbol{h}^t - \boldsymbol{h}^\natural\right\|_2^2 + \left\|\alpha \boldsymbol{x}^t - \boldsymbol{x}^\natural\right\|_2^2. \tag{36}$$

Notably, (35a) naturally leads to the bound on $\left\|\boldsymbol{h}^t\boldsymbol{x}^{t*} - \boldsymbol{h}^\natural\boldsymbol{x}^{\natural*}\right\|_{\mathrm{F}}$. To see this, one can invoke the triangle inequality to obtain

$$\begin{aligned}
\left\|\boldsymbol{h}^t\boldsymbol{x}^{t*} - \boldsymbol{h}^\natural\boldsymbol{x}^{\natural*}\right\|_{\mathrm{F}} &= \left\|\frac{1}{\overline{\alpha^t}}\boldsymbol{h}^t\left(\alpha^t\boldsymbol{x}^t\right)^* - \boldsymbol{h}^\natural\boldsymbol{x}^{\natural*}\right\|_{\mathrm{F}} = \left\|\left(\frac{1}{\overline{\alpha^t}}\boldsymbol{h}^t - \boldsymbol{h}^\natural\right)\left(\alpha^t\boldsymbol{x}^t\right)^* + \boldsymbol{h}^\natural\left(\alpha^t\boldsymbol{x}^t - \boldsymbol{x}^\natural\right)^*\right\|_{\mathrm{F}} \\
&\leq \left\|\left(\frac{1}{\overline{\alpha^t}}\boldsymbol{h}^t - \boldsymbol{h}^\natural\right)\left(\alpha^t\boldsymbol{x}^t\right)^*\right\|_{\mathrm{F}} + \left\|\boldsymbol{h}^\natural\left(\alpha^t\boldsymbol{x}^t - \boldsymbol{x}^\natural\right)^*\right\|_{\mathrm{F}} \\
&\leq \left\|\frac{1}{\overline{\alpha^t}}\boldsymbol{h}^t - \boldsymbol{h}^\natural\right\|_2 \left\|\alpha^t\boldsymbol{x}^t\right\|_2 + \left\|\boldsymbol{h}^\natural\right\|_2 \left\|\alpha^t\boldsymbol{x}^t - \boldsymbol{x}^\natural\right\|_2 \\
&\lesssim \mathrm{dist}\left(\boldsymbol{z}^t, \boldsymbol{z}^\natural\right) \lesssim C_1\left(1 - \frac{\eta}{16}\right)^t \frac{1}{\log^2 m},
\end{aligned}$$

where the last line follows since $\max\left\{\left\|\frac{1}{\overline{\alpha^t}}\boldsymbol{h}^t - \boldsymbol{h}^\natural\right\|_2, \left\|\alpha^t\boldsymbol{x}^t - \boldsymbol{x}^\natural\right\|_2\right\} \leq \mathrm{dist}\left(\boldsymbol{z}^t, \boldsymbol{z}^\natural\right)$ and $\left\|\alpha^t\boldsymbol{x}^t\right\|_2 \leq \left\|\alpha^t\boldsymbol{x}^t - \boldsymbol{x}^\natural\right\|_2 + \left\|\boldsymbol{x}^\natural\right\|_2 \leq 2$.

Theorem 3 provides the first theoretical guarantee of vanilla gradient descent for blind deconvolution at a near-optimal statistical and computational complexity. A few remarks are in order.

- **Implicit regularization:** Theorem 3 reveals that the iterates remain incoherent with the measurement mechanism (see (35b) and (35c)). In particular, we show that it is also unnecessary to regularize the scaling ambiguity, as commonly done. This justifies the use of regularization-free (Wirtinger) gradient descent for blind deconvolution.

- **Constant step size**. Compared to the step size $\eta_t \lesssim 1/m$ suggested in [LLSW16] for regularized gradient descent, our theory admits a substantially more aggressive step size(i.e. $\eta_t \asymp 1$) even without regularization.

Similar to phase retrieval, the computational efficiency is boosted by m times, attaining ϵ-accuracy within $\log(1/\epsilon)$ iterations (vs. $m \log(1/\epsilon)$ iterations in prior theory).

- **Near-optimal sample complexity:** It is demonstrated that vanilla gradient descent succeeds at a near-optimal sample complexity up to logarithmic factors, although our requirement is slightly worse than [LLSW16] which uses explicit regularization. Notably, even under the sample complexity herein, the iteration complexity given in [LLSW16] is still $m/\mathrm{poly}\log(m)$.

- **Incoherence of spectral initialization:** As in phase retrieval, Theorem 3 demonstrates that the estimates returned by the spectral method are incoherent with respect to both $\{\boldsymbol{a}_j\}$ and $\{\boldsymbol{b}_j\}$. In contrast, [LLSW16] recommends a projection operation (via a linear program) to enforce incoherence on the initial estimate, which is dispensable according to our theory.

4 Related work

Solving nonlinear systems of equations has received much attention in the past decade. Rather than directly attacking the nonconvex formulation, convex relaxation lifts the object of interest into a higher dimensional space and then attempts recovery via semidefinite programming (e.g. [RFP10, CSV13, CR09, ARR14]), which has enjoyed great success in both theory and practice. Despite appealing statistical guarantees, semidefinite programming is in general prohibitively expensive when processing large-scale datasets.

Nonconvex approaches, on the other end, have been under extensive study in the last few years, due to their computational advantages. There is a growing list of statistical estimation problems for which nonconvex approaches are guaranteed to find global optimal solutions, including but not limited to phase retrieval [NJS13, CLS15, CC17], low-rank matrix sensing and completion [CW15, ZL15, TBS+16, GLM16], blind deconvolution and self-calibration [LLSW16, LS17, CJ16, LLB17, LLJB17], dictionary learning [SQW17], tensor decomposition [GM17], joint alignment [CC16], learning shallow neural networks [SJL17, ZSJ+17], matrix sensing [TBS+16, BNS16, PKCS16], robust subspace learning [NNS+14, MZL17, CJN17]. In several problems [SQW16, SQW17, GM17, GLM16, LWL+16, LT16, MBM16], it is further suggested that the optimization landscape is benign under sufficiently large sample complexity, in the sense that all local minima are globally optimal, and hence nonconvex iterative algorithms become promising in solving such problems. Below we review the three problems studied in this paper in more details. Some state-of-the-art results are summarized in Table 1.

- *Phase retrieval.* Candès et al. proposed *PhaseLift* [CSV13] to solve the quadratic systems of equations based on convex programming. Specifically, it lifts the decision variable $\boldsymbol{x}^\natural$ into a rank one matrix $\boldsymbol{X}^\natural = \boldsymbol{x}^\natural \boldsymbol{x}^{\natural\top}$ and translates the quadratic constraints of $\boldsymbol{x}^\natural$ in (14) into linear constraints of $\boldsymbol{X}^\natural$. By dropping the rank constraint, the problem becomes convex [CSV13, SESS11, CL14, CCG15, CZ15, Tro15a]. Another convex program PhaseMax [GS16, BR16, HV16, DTL17] operates in the natural parameter space via linear programming, provided that an anchor vector is available. On the other hand, alternating minimization [NJS13] with sample splitting has been shown to enjoy much better computational guarantee. In contrast, Wirtinger Flow [CLS15] provides the first global convergence result for nonconvex methods without sample splitting, whose statistical and computational guarantees are later improved by [CC17] via an adaptive truncation strategy. Several other variants of WF are also proposed [CLM+16, KÖ16, Sol17], among which an amplitude-based loss function has been investigated [WGE17, ZZLC17, WZG+16]. In particular, [ZZLC17] demonstrates that the amplitude-based loss function has a better curvature, and vanilla gradient descent can indeed converge with a constant step size at the order-wise optimal sample complexity. A small sample of other nonconvex phase retrieval methods include [SBE14, CL16, CFL15, DR17, GX16, Wei15, BEB17, TV17, CLW17, QZEW17], which are beyond the scope of this paper.

- *Matrix completion.* Nuclear norm minimization was studied in [CR09] as a convex relaxation paradigm to solve the matrix completion problem. Under certain incoherence conditions imposed upon the ground truth matrix, exact recovery is guaranteed under near-optimal sample complexity [CT10, Gro11, Rec11, Che15]. Concurrently, several works [KMO10a, KMO10b, LB10, JNS13, HW14, HMLZ15, ZWL15, JN15, TW16, JKN16, WCCL16, ZWL15] tackled the matrix completion problem via nonconvex approaches. In particular, the seminal work by Keshavan et al. [KMO10a, KMO10b] pioneered the two-stage approach that is widely adopted by later works. Sun and Luo [SL16] demonstrated the convergence of gradient descent type methods for noiseless matrix completion with a regularized nonconvex loss function. Instead of penalizing the loss function, [CW15, ZL16] employed projection to enforce the incoherence condition throughout the whole trajectory. To the best of our knowledge, no rigorous guarantees have been established for matrix completion without explicit regularization. Our work closes the gap and makes the first contribution towards understanding implicit regularization in vanilla gradient descent method for matrix completion. In addition, near-optimal entrywise eigenvector perturbation has already been studied by [JN15] and [AFWZ17] for matrix completion, which forms the basis for our analysis for spectral initialization.

- *Blind deconvolution.* In [ARR14], Ahmed et al. first proposed to invoke similar lifting idea for blind deconvolution, which translates the bilinear measurements (30) into a system of linear measurements of a rank-one matrix $\boldsymbol{X}^{\natural} = \boldsymbol{h}^{\natural}\boldsymbol{x}^{\natural *}$. Near-optimal performance guarantee have been established for convex relaxation [ARR14]. Under the same model, Li et al. [LLSW16] proposed a regularized gradient descent algorithm that directly optimizes the nonconvex loss function (31) with a few regularization terms that account for scaling ambiguity and incoherence. See [CJ16] for a related formulation. In [HH17], a Riemannian steepest descent method is developed that removes the regularization for scaling ambiguity, although they still need to regularize for incoherence. In [AAH17], a linear program is proposed but requires exact knowledge of the signs of the signals. Blind deconvolution has also been studied for other models – interested readers may refer to [Chi16, LS17, LLJB17, LS15, LTR16, ZLK+17].

On the other hand, our analysis framework is based on a leave-one-out perturbation argument. This technique has been widely used to analyze high-dimensional problems with random designs, including but not limited to robust M-estimation [EKBB+13, EK15], statistical inference for sparse regression [JM15], likelihood ratio test in logistic regression [SCC17], phase synchronization [ZB17, AFWZ17], ranking from pairwise comparisons [CFMW17], community recovery [AFWZ17], and recovering structured probability matrices [Che17]. In particular, this technique results in tight performance guarantees for the generalized power method [ZB17], the spectral method [AFWZ17, CFMW17], and convex programming approaches [EK15, ZB17, SCC17, CFMW17], although it has never been applied to analyze nonconvex optimization algorithms.

Finally, we note that the notion of implicit regularization — broadly defined — comes up in settings far beyond the models and algorithms considered herein. For instance, it has been discovered that in matrix factorization, over-parameterized stochastic gradient descent effectively enforces certain norm constraints, allowing it to converge to a minimal-norm solution as long as it starts from the origin [GWB+17]. The stochastic gradient methods have also been shown to implicitly enforce Tikhonov regularization in several statistical learning settings [LCR16]. More broadly, this phenomenon is even crucial in enabling efficient training of deep neural networks [NTS14, NTSS17, ZBH+16, SHS17, KMN+16].

5 A general recipe for trajectory analysis

In this section, we sketch a general recipe for establishing performance guarantees of gradient descent, which contains the key idea for proving the main results of this paper. The main challenge is to demonstrate that appropriate incoherence conditions are preserved throughout the entire trajectory of the algorithm. This requires exploiting statistical independence of the samples in a careful manner, in conjunction with generic optimization theory. Central to our approach is a leave-one-out perturbation argument, which allows to decouple the statistical dependency while controlling the component-wise incoherence measures.

5.1 General model

Consider the following problem where the samples are collected in a bilinear/quadratic form as

$$y_j = \boldsymbol{\psi}_j^* \boldsymbol{H}^{\natural} \boldsymbol{X}^{\natural *} \boldsymbol{\phi}_j, \qquad 1 \le j \le m, \tag{37}$$

where the objects of interest $\boldsymbol{H}^{\natural}, \boldsymbol{X}^{\natural} \in \mathbb{C}^{n\times r}$ or $\mathbb{R}^{n\times r}$ might be vectors or tall matrices taking either real or complex values. The design vectors $\{\boldsymbol{\psi}_j\}$ and $\{\boldsymbol{\phi}_j\}$ are in either $\mathbb{C}^n$ or $\mathbb{R}^n$, and can be either random or deterministic. This model is quite general and entails all three examples as special cases:

- *Phase retrieval*: $\boldsymbol{H}^\natural = \boldsymbol{X}^\natural = \boldsymbol{x}^\natural \in \mathbb{R}^{n\times 1}$, and $\boldsymbol{\psi}_j = \boldsymbol{\phi}_j = \boldsymbol{a}_j$;
- *Matrix completion*: $\boldsymbol{H}^\natural = \boldsymbol{X}^\natural \in \mathbb{R}^{n\times r}$ and $\boldsymbol{\psi}_j, \boldsymbol{\phi}_j \in \{\boldsymbol{e}_1, \cdots, \boldsymbol{e}_n\}$;
- *Blind deconvolution*: $\boldsymbol{H}^\natural = \boldsymbol{h}^\natural \in \mathbb{C}^K$, $\boldsymbol{X}^\natural = \boldsymbol{x}^\natural \in \mathbb{C}^K$, $\boldsymbol{\phi}_j = \boldsymbol{a}_j$, and $\boldsymbol{\psi}_j = \boldsymbol{b}_j$.

For this setting, the empirical loss function is given by

$$f(\boldsymbol{Z}) := f(\boldsymbol{H}, \boldsymbol{X}) = \frac{1}{m}\sum_{j=1}^m \left|\boldsymbol{\psi}_j^* \boldsymbol{H}\boldsymbol{X}^* \boldsymbol{\phi}_j - y_j\right|^2.$$

To minimize $f(\boldsymbol{Z})$, we proceed with vanilla gradient descent

$$\boldsymbol{Z}^{t+1} = \boldsymbol{Z}^t - \eta \nabla f\big(\boldsymbol{Z}^t\big), \qquad \forall t \geq 0$$

following a standard spectral initialization, where η is the step size. As a remark, for complex-valued problems, the gradient (resp. Hessian) should be understood as the Wirtinger gradient (resp. Hessian).

It is clear from (37) that $\boldsymbol{Z}^\natural = (\boldsymbol{H}^\natural, \boldsymbol{X}^\natural)$ can only be recovered up to certain global ambiguity. For clarity of presentation, we assume in this section that such ambiguity has already been taken care of via proper transformation.

5.2 Outline of the recipe

We are now positioned to outline the general recipe, which have the following steps.

- **Step 1: characterizing local geometry in the RIC.** Our first step is to characterize a region $\mathcal{R}$ — which we term as the *region of incoherence and contraction* (RIC) — such that the Hessian matrix $\nabla^2 f(\boldsymbol{Z})$ obeys strong convexity and smoothness,

$$\boldsymbol{0} \prec \alpha \boldsymbol{I} \preceq \nabla^2 f(\boldsymbol{Z}) \preceq \beta \boldsymbol{I}, \qquad \forall \boldsymbol{Z} \in \mathcal{R}, \tag{38}$$

  or at least along certain directions (i.e. restricted strong convexity and smoothness), where β/α scales slowly (or even remains bounded) with the problem size. As revealed by optimization theory, this geometry (38) immediately implies linear convergence with the contraction rate $1 - O(\alpha/\beta)$ for a properly chosen step size η, as long as all iterates stay within the RIC.

  A natural question then arises: what does the RIC $\mathcal{R}$ look like? As it turns out, the RIC typically contains all points such that the ℓ_2 error $\|\boldsymbol{Z} - \boldsymbol{Z}^\natural\|_{\mathrm{F}}$ is not too large and

$$(\textbf{incoherence}) \qquad \max_j \left\|\boldsymbol{\phi}_j^*(\boldsymbol{X} - \boldsymbol{X}^\natural)\right\|_2 \text{ and } \max_j \left\|\boldsymbol{\psi}_j^*(\boldsymbol{H} - \boldsymbol{H}^\natural)\right\|_2 \text{ are well-controlled.} \tag{39}$$

  In the three examples, the above incoherence condition translates to:

  - *Phase retrieval*: $\max_{1\leq j\leq m} \left|\boldsymbol{a}_j^\top(\boldsymbol{x} - \boldsymbol{x}^\natural)\right|$ is well-controlled;
  - *Matrix completion*: $\left\|\boldsymbol{X} - \boldsymbol{X}^\natural\right\|_{2,\infty}$ is well-controlled;
  - *Blind deconvolution*: $\max_{1\leq j\leq m} \left|\boldsymbol{a}_j^\top(\boldsymbol{x} - \boldsymbol{x}^\natural)\right|$ and $\max_{1\leq j\leq m} \left|\boldsymbol{b}_j^\top(\boldsymbol{h} - \boldsymbol{h}^\natural)\right|$ are well-controlled.

- **Step 2: introducing the leave-one-out sequences.** To justify that no iterates leave the RIC, we rely on auxiliary sequences. Specifically, for each l, construct an auxiliary sequence $\{\boldsymbol{Z}^{t,(l)} = (\boldsymbol{X}^{t,(l)}, \boldsymbol{H}^{t,(l)})\}$ such that $\boldsymbol{X}^{t,(l)}$ (resp. $\boldsymbol{H}^{t,(l)}$) is independent of any sample involving $\boldsymbol{\phi}_l$ (resp. $\boldsymbol{\psi}_l$). As an example, suppose that the $\boldsymbol{\phi}_l$'s and the $\boldsymbol{\psi}_l$'s are independently and randomly generated. Then for each l, one can consider a leave-one-out loss function

$$f^{(l)}(\boldsymbol{Z}) := \frac{1}{m}\sum_{j:j\neq l} \left|\boldsymbol{\psi}_j^* \boldsymbol{H}\boldsymbol{X}^* \boldsymbol{\phi}_j - y_j\right|^2$$

  that discards the lth sample, and generate $\{\boldsymbol{Z}^{t,(l)}\}$ by running vanilla GD w.r.t. this auxiliary loss function, with a spectral initialization that similarly discards the lth sample. Note that this procedure is only introduced to facilitate analysis and never implemented in practice.

- **Step 3: establishing the incoherence condition.** We are now ready to establish the incoherence condition with the help of the auxiliary sequences. Usually the proof proceeds by induction, where our goal is to show the next iterate still lies within the RIC, given that the current one does.
  - **Step 3(a): proximity between the original and the leave-one-out iterates.** As one can anticipate, $\{\boldsymbol{Z}^t\}$ and $\{\boldsymbol{Z}^{t,(l)}\}$ remain "glued" to each other along the whole trajectory, since their constructions differ by only a single sample. In fact, as long as the initializations stay sufficiently close, their gaps will never explode. To intuitively see why, use the fact $\nabla f(\boldsymbol{Z}^t) \approx \nabla f^{(l)}(\boldsymbol{Z}^t)$ to discover that

$$\begin{aligned}\boldsymbol{Z}^{t+1} - \boldsymbol{Z}^{t+1,(l)} &= \boldsymbol{Z}^{t+1} - \eta \nabla f(\boldsymbol{Z}^t) - \big(\boldsymbol{Z}^{t+1,(l)} - \eta \nabla f^{(l)}\big(\boldsymbol{Z}^{t,(l)}\big)\big) \\ &\approx \boldsymbol{Z}^t - \boldsymbol{Z}^{t,(l)} - \eta \nabla^2 f(\boldsymbol{Z}^t)\big(\boldsymbol{Z}^t - \boldsymbol{Z}^{t,(l)}\big),\end{aligned}$$

    which together with the strong convexity condition implies ℓ_2 contraction

$$\big\|\boldsymbol{Z}^{t+1} - \boldsymbol{Z}^{t+1,(l)}\big\|_{\mathrm{F}} \approx \Big\|\big(\boldsymbol{I} - \eta \nabla^2 f(\boldsymbol{Z}^t)\big)\big(\boldsymbol{Z}^t - \boldsymbol{Z}^{t,(l)}\big)\Big\|_{\mathrm{F}} \le \big\|\boldsymbol{Z}^t - \boldsymbol{Z}^{t,(l)}\big\|_2.$$

    Indeed, (restricted) strong convexity is crucial in controlling the size of leave-one-out perturbations.
  - **Step 3(b): incoherence condition of the leave-one-out iterates.** The fact that $\boldsymbol{Z}^{t+1}$ and $\boldsymbol{Z}^{t+1,(l)}$ are exceedingly close motivates us to control the incoherence of $\boldsymbol{Z}^{t+1,(l)}$ instead, for $1 \le l \le m$. By construction, $\boldsymbol{X}^{t+1,(l)}$ (resp. $\boldsymbol{H}^{t+1,(l)}$) is statistically *independent* of any sample involving the design vector $\boldsymbol{\phi}_l$ (resp. $\boldsymbol{\psi}_l$), a fact that typically leads to a more friendly analysis for controlling $\boldsymbol{\phi}_l^*\big(\boldsymbol{X}^{t+1,(l)} - \boldsymbol{X}^\natural\big)$ and $\boldsymbol{\psi}_l^*\big(\boldsymbol{H}^{t+1,(l)} - \boldsymbol{H}^\natural\big)$.
  - **Step 3(c): combining the bounds.** With these results in place, apply the triangle inequality to obtain

$$\big\|\boldsymbol{\phi}_l^*\big(\boldsymbol{X}^{t+1} - \boldsymbol{X}^\natural\big)\big\|_2 \le \|\boldsymbol{\phi}_l\|_2 \big\|\boldsymbol{X}^{t+1} - \boldsymbol{X}^{t+1,(l)}\big\|_{\mathrm{F}} + \big\|\boldsymbol{\phi}_l^*\big(\boldsymbol{X}^{t+1,(l)} - \boldsymbol{X}^\natural\big)\big\|_2,$$

    where the first term is controlled in Step 3(a) and the second term is controlled in Step 3(b). The term $\big\|\boldsymbol{\psi}_l^*\big(\boldsymbol{H}^{t+1} - \boldsymbol{H}^\natural\big)\big\|_2$ can be bounded similarly. By choosing the bounds properly, this establishes the incoherence condition for all $1 \le l \le m$ as desired.

General Recipe (a leave-one-out analysis)

Step 1: characterize restricted strong convexity and local smoothness of f, and identify the region of incoherence and contraction (RIC).

Step 2: introduce leave-one-out sequences $\{\boldsymbol{X}^{t,(l)}\}$ and $\{\boldsymbol{H}^{t,(l)}\}$ for each l, where $\{\boldsymbol{X}^{t,(l)}\}$ (resp. $\{\boldsymbol{H}^{t,(l)}\}$) is independent of any sample involving $\boldsymbol{\phi}_l$ (resp. $\boldsymbol{\psi}_l$);

Step 3: establish the incoherence condition of $\{\boldsymbol{X}^t\}$ and $\{\boldsymbol{H}^t\}$ via induction. Suppose the iterates satisfy the claimed conditions in the tth iteration:

(a) show, via restricted strong convexity, that the true iterates $(\boldsymbol{X}^{t+1}, \boldsymbol{H}^{t+1})$ and the leave-one-out version $(\boldsymbol{X}^{t+1,(l)}, \boldsymbol{H}^{t+1,(l)})$ are exceedingly close;

(b) use statistical independence to show that $\boldsymbol{X}^{t+1,(l)}$ (resp. $\boldsymbol{H}^{t+1,(l)}$) is incoherent w.r.t. $\boldsymbol{\phi}_l$ (resp. $\boldsymbol{\psi}_l$), namely, $\|\boldsymbol{\phi}_l^*\boldsymbol{X}^{t+1,(l)}\|_2$ and $\|\boldsymbol{\psi}_l^*\boldsymbol{H}^{t+1,(l)}\|_2$ are both well-controlled;

(c) combine the bounds to establish the desired incoherence condition by showing that $\|\boldsymbol{\phi}_l^*\boldsymbol{X}^{t+1,(l)}\|_2 \approx \|\boldsymbol{\phi}_l^*\boldsymbol{X}^{t+1}\|_2$ and $\|\boldsymbol{\psi}_l^*\boldsymbol{H}^{t+1}\|_2 \approx \|\boldsymbol{\psi}_l^*\boldsymbol{H}^{t+1,(l)}\|_2$.

6 Analysis for phase retrieval

In this section, we instantiate the general recipe presented in Section 5 to phase retrieval and prove Theorem 1. Without loss of generality, we assume throughout this section that $\big\|\boldsymbol{x}^\natural\big\|_2 = 1$ and

$$\mathrm{dist}(\boldsymbol{x}^0, \boldsymbol{x}^\natural) = \|\boldsymbol{x}^0 - \boldsymbol{x}^\natural\|_2 \le \|\boldsymbol{x}^0 + \boldsymbol{x}^\natural\|_2. \tag{40}$$

In addition, the gradient and the Hessian of $f(\cdot)$ for this problem (see (15)) are given respectively by

$$\nabla f(\boldsymbol{x}) = \frac{1}{m}\sum_{j=1}^{m}\left[\left(\boldsymbol{a}_j^{\top}\boldsymbol{x}\right)^2 - y_j\right]\left(\boldsymbol{a}_j^{\top}\boldsymbol{x}\right)\boldsymbol{a}_j, \tag{41}$$

$$\nabla^2 f(\boldsymbol{x}) = \frac{1}{m}\sum_{j=1}^{m}\left[3\left(\boldsymbol{a}_j^{\top}\boldsymbol{x}\right)^2 - y_j\right]\boldsymbol{a}_j\boldsymbol{a}_j^{\top}, \tag{42}$$

which are useful throughout the proof.

6.1 Step 1: characterizing local geometry in the RIC

6.1.1 Local geometry

We start by characterizing the region that enjoys both strong convexity and the desired level of smoothness. This is supplied in the following lemma, which plays a crucial role in the subsequent analysis.

Lemma 1 (Restricted strong convexity and smoothness for phase retrieval)**.** *Fix any sufficiently small constant $C_1 > 0$ and any sufficiently large constant $C_2 > 0$, and suppose the sample complexity obeys $m \geq c_0 n \log n$ for some sufficiently large constant $c_0 > 0$. With probability at least $1 - O(mn^{-10})$,*

$$\nabla^2 f(\boldsymbol{x}) \succeq \frac{1}{2}\boldsymbol{I}_n$$

holds simultaneously for all $\boldsymbol{x} \in \mathbb{R}^n$ satisfying $\left\|\boldsymbol{x} - \boldsymbol{x}^{\natural}\right\|_2 \leq 2C_1$; and

$$\nabla^2 f(\boldsymbol{x}) \preceq \left(5C_2\left(10 + C_2\right)\log n\right)\boldsymbol{I}_n$$

holds simultaneously for all $\boldsymbol{x} \in \mathbb{R}^n$ obeying

$$\left\|\boldsymbol{x}^t - \boldsymbol{x}^{\natural}\right\|_2 \leq 2C_1, \tag{43a}$$

$$\max_{1\leq j\leq m}\left|\boldsymbol{a}_j^{\top}\left(\boldsymbol{x}^t - \boldsymbol{x}^{\natural}\right)\right| \leq C_2\sqrt{\log n}. \tag{43b}$$

Proof. See Appendix A.1. □

In words, Lemma 1 reveals that the Hessian matrix is positive definite and (almost) well-conditioned, if one restricts attention to the set of points in a local region that are (i) not far away from the truth (cf. (43a)) and that (ii) remain incoherent with respect to the sampling vectors $\{\boldsymbol{a}_j\}_{1\leq j\leq m}$ (cf. (43b)).

6.1.2 The RIC and ℓ_2 error contraction

As we point out before, the nice local geometry enables ℓ_2 contraction, which we formalize below.

Lemma 2. *With probability exceeding $1 - O(mn^{-10})$, one has*

$$\left\|\boldsymbol{x}^{t+1} - \boldsymbol{x}^{\natural}\right\|_2 \leq (1 - \eta/2)\left\|\boldsymbol{x}^t - \boldsymbol{x}^{\natural}\right\|_2 \tag{44}$$

for all $t \geq 0$ obeying the condition (43) or satisfying $\|\boldsymbol{x}^t - \boldsymbol{x}^{\natural}\|_2 \leq \frac{1}{n}\|\boldsymbol{x}^{\natural}\|_2$, provided that the step size satisfies $0 < \eta \leq \frac{1}{5C_2(10+C_2)\log n}$.

Proof. This proof applies the standard argument when establishing the ℓ_2 error contraction of gradient descent for strongly convex and smooth functions. See Appendix A.2. □

With the help of Lemma 2, we can turn the proof of Theorem 1 into ensuring that the trajectory $\{\boldsymbol{x}^t\}$ up to $t = T_0 = n$ lies in the good region[9] specified by (45). This is formally stated in the next lemma.

[9]Note that we deliberately change $2C_1$ in (43a) to C_1 in the definition of the RIC (45a) to ensure the correctness of the analysis.

Algorithm 4 The lth leave-one-out sequence for phase retrieval

Input: $\{\boldsymbol{a}_j\}_{1\le j\le m, j\ne l}$ and $\{y_j\}_{1\le j\le m, j\ne l}$.

Spectral initialization: let $\lambda_1\big(\boldsymbol{Y}^{(l)}\big)$ and $\tilde{\boldsymbol{x}}^{0,(l)}$ be the leading eigenvalue and eigenvector of

$$\boldsymbol{Y}^{(l)} = \frac{1}{m}\sum_{j:j\ne l} y_j \boldsymbol{a}_j\boldsymbol{a}_j^\top,$$

respectively, and set

$$\boldsymbol{x}^{0,(l)} = \begin{cases} \sqrt{\lambda_1\left(\boldsymbol{Y}^{(l)}\right)/3}\,\tilde{\boldsymbol{x}}^{0,(l)}, & \text{if } \big\|\tilde{\boldsymbol{x}}^{0,(l)} - \boldsymbol{x}^\natural\big\|_2 \le \big\|\tilde{\boldsymbol{x}}^{0,(l)} + \boldsymbol{x}^\natural\big\|_2, \\ -\sqrt{\lambda_1\left(\boldsymbol{Y}^{(l)}\right)/3}\,\tilde{\boldsymbol{x}}^{0,(l)}, & \text{else.} \end{cases}$$

Gradient updates: **for** $t = 0, 1, 2, \ldots, T-1$ **do**

$$\boldsymbol{x}^{t+1,(l)} = \boldsymbol{x}^{t,(l)} - \eta_t \nabla f^{(l)}\big(\boldsymbol{x}^{t,(l)}\big). \tag{48}$$

Lemma 3. *Suppose for all $0 \le t \le T_0 := n$, the trajectory $\{\boldsymbol{x}^t\}$ falls within the nice region (termed the RIC), namely,*

$$\big\|\boldsymbol{x}^t - \boldsymbol{x}^\natural\big\|_2 \le C_1, \tag{45a}$$

$$\max_{1\le l\le m}\left|\boldsymbol{a}_l^\top\left(\boldsymbol{x}^t - \boldsymbol{x}^\natural\right)\right| \le C_2\sqrt{\log n}, \tag{45b}$$

then the claims in Theorem 1 hold true.

Proof. See Appendix A.3. □

6.2 Step 2: introducing the leave-one-out sequences

6.2.1 Leave-one-out sequences

In comparison to the ℓ_2 error bound (45a) that captures the overall loss, the incoherence hypothesis (45b) — which concerns sample-wise control of the empirical risk — is more complicated to establish, partly due to the statistical dependence between $\boldsymbol{x}^t$ and the sampling vectors $\boldsymbol{a}_l$'s. As described in the general recipe, the key idea is the introduction of a *leave-one-out* version of the WF iterates, which removes a single measurement from consideration.

To be precise, for each $1 \le l \le m$, we define the leave-one-out empirical loss function as

$$f^{(l)}(\boldsymbol{x}) := \frac{1}{4m}\sum_{j:j\ne l}\Big[\big(\boldsymbol{a}_j^\top\boldsymbol{x}\big)^2 - y_j\Big]^2, \tag{46}$$

and the auxiliary trajectory $\big\{\boldsymbol{x}^{t,(l)}\big\}_{t\ge 0}$ is constructed by running WF w.r.t. $f^{(l)}(\boldsymbol{x})$. In addition, the spectral initialization $\boldsymbol{x}^{0,(l)}$ is computed based on the rescaled leading eigenvector of the leave-one-out data matrix

$$\boldsymbol{Y}^{(l)} := \frac{1}{m}\sum_{j:j\ne l} y_j\boldsymbol{a}_j\boldsymbol{a}_j^\top. \tag{47}$$

Clearly, the entire sequence $\big\{\boldsymbol{x}^{t,(l)}\big\}_{t\ge 0}$ is independent of the lth sampling vector $\boldsymbol{a}_l$. This auxiliary procedure is formally described in Algorithm 4.

6.2.2 Induction hypotheses

Our proof will be inductive in nature. For the sake of clarity, we list all the induction hypotheses, one of which is pertinent to the leave-one-out sequences (first-time readers can skip these):

$$\big\|\boldsymbol{x}^t - \boldsymbol{x}^\natural\big\|_2 \le C_1, \tag{49a}$$

$$\max_{1\le l\le m}\left\|\boldsymbol{x}^t-\boldsymbol{x}^{t,(l)}\right\|_2\le C_3\sqrt{\frac{\log n}{n}} \tag{49b}$$

$$\max_{1\le j\le m}\left|\boldsymbol{a}_j^\top\left(\boldsymbol{x}^t-\boldsymbol{x}^\natural\right)\right|\le C_2\sqrt{\log n}. \tag{49c}$$

The induction on (49a), that is,

$$\left\|\boldsymbol{x}^{t+1}-\boldsymbol{x}^\natural\right\|_2\le C_1, \tag{50}$$

has already been established in Lemma 2. Hence our focus will be on (49b) and (49c) in the next subsection. We defer justification of the base case (i.e. (49) with $t=0$) to Section 6.4.

6.3 Step 3: establishing the incoherence condition

As revealed by Lemma 3, it suffices to prove that the iterates $\{\boldsymbol{x}^t\}_{0\le t\le T_0}$ satisfies (45). This subsection is devoted to establishing (49b) and (49c) for $t+1$, assuming that (49) holds true for t.

- **Step 3(a): proximity between the original and the leave-one-out iterates.** The leave-one-out sequence $\{\boldsymbol{x}^{t,(l)}\}$ behaves similarly to the true WF iterates while maintaining statistical independence with $\boldsymbol{a}_l$, a key fact that allows us to control the incoherence of lth leave-one-out sequence w.r.t. $\boldsymbol{a}_l$. We will formally quantify the gap between $\boldsymbol{x}^{t+1}$ and $\boldsymbol{x}^{t+1,(l)}$ in the following lemma.

  Lemma 4. *Under the hypotheses (49), with probability at least* $1-O(mn^{-10})$,

  $$\max_{1\le l\le m}\left\|\boldsymbol{x}^{t+1}-\boldsymbol{x}^{t+1,(l)}\right\|_2\le C_3\sqrt{\frac{\log n}{n}}. \tag{51}$$

  Proof. The proof relies heavily on restricted strong convexity and is deferred to Appendix A.4. □

- **Step 3(b): incoherence of the leave-one-out iterates.** By construction, $\boldsymbol{x}^{t+1,(l)}$ is statistically independent of the sampling vector $\boldsymbol{a}_l$. One can thus invoke the standard Gaussian concentration results to derive that with probability at least $1-O\left(mn^{-10}\right)$,

  $$\begin{aligned}\max_{1\le l\le m}\left|\boldsymbol{a}_l^\top\left(\boldsymbol{x}^{t+1,(l)}-\boldsymbol{x}^\natural\right)\right| &\le 5\sqrt{\log n}\left\|\boldsymbol{x}^{t+1,(l)}-\boldsymbol{x}^\natural\right\|_2\\ &\overset{\text{(i)}}{\le} 5\sqrt{\log n}\left(\left\|\boldsymbol{x}^{t+1,(l)}-\boldsymbol{x}^{t+1}\right\|_2+\left\|\boldsymbol{x}^{t+1}-\boldsymbol{x}^\natural\right\|_2\right)\\ &\overset{\text{(ii)}}{\le} 5\sqrt{\log n}\left(C_3\sqrt{\frac{\log n}{n}}+C_1\right)\\ &\le C_4\sqrt{\log n}\end{aligned} \tag{52}$$

  holds for some sufficiently large constant $C_4\ge 6C_1>0$. Here, (i) comes from the triangle inequality, and (ii) arises from the proximity bound (51) and the condition (50).

- **Step 3(c): combining the bounds.** We are now prepared to establish (45b) for $t+1$. Specifically,

  $$\begin{aligned}\max_{1\le l\le m}\left|\boldsymbol{a}_l^\top\left(\boldsymbol{x}^{t+1}-\boldsymbol{x}^\natural\right)\right| &\le \max_{1\le l\le m}\left|\boldsymbol{a}_l^\top\left(\boldsymbol{x}^{t+1}-\boldsymbol{x}^{t+1,(l)}\right)\right|+\max_{1\le l\le m}\left|\boldsymbol{a}_l^\top\left(\boldsymbol{x}^{t+1,(l)}-\boldsymbol{x}^\natural\right)\right|\\ &\overset{\text{(i)}}{\le} \max_{1\le l\le m}\|\boldsymbol{a}_l\|_2\left\|\boldsymbol{x}^{t+1}-\boldsymbol{x}^{t+1,(l)}\right\|_2+C_4\sqrt{\log n}\\ &\overset{\text{(ii)}}{\le} \sqrt{6n}\cdot C_3\sqrt{\frac{\log n}{n}}+C_4\sqrt{\log n}\le C_2\sqrt{\log n},\end{aligned} \tag{53}$$

  where (i) follows from the Cauchy-Schwarz inequality and (52), the inequality (ii) is a consequence of (51) and Lemma 33, and the last inequality holds as long as $C_2/(C_3+C_4)$ is sufficiently large.

Using mathematical induction and the union bound, we establish (49) for all $t\le T_0=n$ with very high probability. This in turn concludes the proof of Theorem 1, as long as the hypotheses are valid for the base case.

6.4 The base case

In the end, we return to verify the base case, i.e. the spectral initialization obeys (49) with $t = 0$. The following lemma justifies (49a) by choosing δ sufficiently small.

Lemma 5. *Fix any small constant $\delta > 0$, and suppose $m > c_0 n \log n$ for some large constant $c_0 > 0$. Consider the two vectors $\boldsymbol{x}^0$ and $\tilde{\boldsymbol{x}}^0$ as defined in Algorithm 1, and suppose without loss of generality that (40) holds. Then with probability exceeding $1 - O(n^{-10})$, one has*

$$\|\boldsymbol{Y} - \mathbb{E}[\boldsymbol{Y}]\| \leq \delta, \tag{54}$$

$$\|\boldsymbol{x}^0 - \boldsymbol{x}^\natural\|_2 \leq 2\delta \qquad \text{and} \qquad \left\|\tilde{\boldsymbol{x}}^0 - \boldsymbol{x}^\natural\right\|_2 \leq \sqrt{2}\delta. \tag{55}$$

Proof. This result follows directly from the Davis-Kahan sinΘ theorem. See Appendix A.5. □

We then move on to check the proximity between the original and leave-one-out iterates for $t = 0$.

Lemma 6. *Suppose $m > c_0 n \log n$ for some large constant $c_0 > 0$. Then with probability at least $1 - O(n^{-10})$, one has*

$$\max_{1 \leq l \leq m} \left\|\boldsymbol{x}^0 - \boldsymbol{x}^{0,(l)}\right\|_2 \leq C_3 \sqrt{\frac{\log n}{n}}. \tag{56}$$

Proof. See Appendix A.6. □

The final claim (49c) can be proved using the same argument as in deriving (53), and hence is omitted.

7 Analysis for matrix completion

This section is devoted to proving Theorem 2. Throughout the proof, we assume that the sample size and noise satisfy

$$n^2 p \gtrsim \mu^3 r^3 n \log^3 n \qquad \text{and} \qquad \sigma \sqrt{\frac{n}{p}} \lesssim \frac{\sigma_{\min}}{\sqrt{\kappa^3 \mu r \log^3 n}},$$

where $\sigma_{\min}$ is the least singular value of $\boldsymbol{M}^\natural$. Before continuing, we first gather a few useful facts.

7.1 Preliminaries and notations

The gradient of the function f defined in (22) is given by

$$\nabla f(\boldsymbol{X}) = \frac{1}{p} \mathcal{P}_\Omega \left[\boldsymbol{X}\boldsymbol{X}^\top - \left(\boldsymbol{M}^\natural + \boldsymbol{E}\right)\right] \boldsymbol{X}. \tag{57}$$

We also define the expected gradient (with respect to the sampling set) to be

$$\nabla F(\boldsymbol{X}) = \left[\boldsymbol{X}\boldsymbol{X}^\top - \left(\boldsymbol{M}^\natural + \boldsymbol{E}\right)\right] \boldsymbol{X}.$$

For notational simplicity, we define the (expected) gradient without noise as

$$\nabla f_{\text{clean}}(\boldsymbol{X}) = \frac{1}{p} \mathcal{P}_\Omega \left(\boldsymbol{X}\boldsymbol{X}^\top - \boldsymbol{M}^\natural\right) \boldsymbol{X} \qquad \text{and} \qquad \nabla F_{\text{clean}}(\boldsymbol{X}) = \left(\boldsymbol{X}\boldsymbol{X}^\top - \boldsymbol{M}^\natural\right) \boldsymbol{X}.$$

Clearly we have the relationship that

$$\nabla f(\boldsymbol{X}) = \nabla f_{\text{clean}}(\boldsymbol{X}) - \frac{1}{p} \mathcal{P}_\Omega(\boldsymbol{E}) \boldsymbol{X} \qquad \text{and} \qquad \nabla F(\boldsymbol{X}) = \nabla F_{\text{clean}}(\boldsymbol{X}) - \boldsymbol{E}\boldsymbol{X}. \tag{58}$$

We also need the Hessian $\nabla^2 f_{\text{clean}}(\boldsymbol{X})$. Note that $\nabla^2 f_{\text{clean}}(\boldsymbol{X})$ needs to be represented by an $nr \times nr$ matrix. Some simple calculation reveals that for any $\boldsymbol{V} \in \mathbb{R}^{n \times r}$,

$$\text{vec}(\boldsymbol{V})^\top \nabla^2 f_{\text{clean}}(\boldsymbol{X}) \, \text{vec}(\boldsymbol{V}) = \frac{1}{2p} \left\|\mathcal{P}_\Omega \left(\boldsymbol{V}\boldsymbol{X}^\top + \boldsymbol{X}\boldsymbol{V}^\top\right)\right\|_{\text{F}}^2 + \frac{1}{p} \left\langle \mathcal{P}_\Omega \left(\boldsymbol{X}\boldsymbol{X}^\top - \boldsymbol{M}^\natural\right), \boldsymbol{V}\boldsymbol{V}^\top \right\rangle, \tag{59}$$

where $\text{vec}(\boldsymbol{V}) \in \mathbb{R}^{nr}$ denotes the vectorization of $\boldsymbol{V}$.

7.2 Step 1: characterizing local geometry in the RIC

7.2.1 Local geometry

As suggested by the general recipe, the first step is to characterize restricted strong convexity and smoothness of the empirical loss function near $\boldsymbol{X}^\natural$.

Lemma 7 (Restricted strong convexity and smoothness for matrix completion)**.** *Suppose that the sample size exceeds $n^2 p \geq C\kappa\mu r n \log n$ for some sufficiently large constant $C > 0$. Then with probability at least $1 - O\left(n^{-10}\right)$, the Hessian $\nabla^2 f_{\mathrm{clean}}(\boldsymbol{X})$ as defined in Section 7.1 obeys*

$$\mathrm{vec}\left(\boldsymbol{V}\right)^\top \nabla^2 f_{\mathrm{clean}}\left(\boldsymbol{X}\right) \mathrm{vec}\left(\boldsymbol{V}\right) \geq \frac{1}{2}\sigma_{\min} \left\|\boldsymbol{V}\right\|_{\mathrm{F}}^2 \qquad \text{and} \qquad \left\|\nabla^2 f_{\mathrm{clean}}\left(\boldsymbol{X}\right)\right\| \leq \frac{5}{2}\sigma_{\max} \tag{60}$$

for all $\boldsymbol{X}$ and $\boldsymbol{V}$ satisfying the following conditions:

- $\left\|\boldsymbol{X} - \boldsymbol{X}^\natural\right\|_{2,\infty} \leq \epsilon \left\|\boldsymbol{X}^\natural\right\|_{2,\infty}$ *with* $\epsilon \ll 1/\sqrt{\kappa^3 \mu r \log^2 n}$*;*
- $\boldsymbol{V} = \boldsymbol{Y}\boldsymbol{H}_Y - \boldsymbol{Z}$ *for some* $\boldsymbol{Y}$ *and* $\boldsymbol{Z}$ *obeying* $\max\{\|\boldsymbol{Y} - \boldsymbol{X}^\natural\|, \|\boldsymbol{Z} - \boldsymbol{X}^\natural\|\} \leq \delta \|\boldsymbol{X}^\natural\|$*, with* $\kappa\delta \ll 1$*, where* $\boldsymbol{H}_Y := \arg\min_{\boldsymbol{R} \in \mathcal{O}^{r\times r}} \|\boldsymbol{Y}\boldsymbol{R} - \boldsymbol{Z}\|_{\mathrm{F}}$.

Proof. See Appendix B.1. □

Remark 4. The second condition regarding $\boldsymbol{V}$ is characterized using the spectral norm $\|\cdot\|$, while in previous works this is typically presented in the Frobenius norm. It is worth noting that the Hessian matrix — even in the infinite-sample and noiseless case — is rank-deficient and cannot be positive definite. As a result, we resort to the form of strong convexity in (60) by restricting attention to certain directions.

7.2.2 Error contraction

Our goal is to demonstrate the error bounds (27) measured by three different norms. Notably, as long as the iterates satisfy (27) at the tth iteration, then $\left\|\boldsymbol{X}^t \hat{\boldsymbol{H}}^t - \boldsymbol{X}^\natural\right\|_{2,\infty}$ is sufficiently small, where $\hat{\boldsymbol{H}}^t$ is as defined in (25). Under our sample complexity assumption, $\boldsymbol{X}^t \hat{\boldsymbol{H}}^t$ satisfies the ℓ_2/ℓ_∞ condition required in Lemma 7. Consequently, we can invoke Lemma 7 to arrive at the following error contraction result.

Lemma 8 (Contraction w.r.t. $\|\cdot\|_{\mathrm{F}}$)*. Suppose the sample complexity obeys $n^2 p \geq C\kappa^3\mu^3 r^3 n \log^3 n$ and the noise satisfies* (26)*. If the iterates satisfy* (27) *at the tth iteration, then with probability at least $1 - O(n^{-10})$,*

$$\left\|\boldsymbol{X}^{t+1}\hat{\boldsymbol{H}}^{t+1} - \boldsymbol{X}^\natural\right\|_{\mathrm{F}} \leq C_4 \rho^{t+1} \mu r \frac{1}{\sqrt{np}} \left\|\boldsymbol{X}^\natural\right\|_{\mathrm{F}} + C_1 \frac{\sigma}{\sigma_{\min}} \sqrt{\frac{n}{p}} \left\|\boldsymbol{X}^\natural\right\|_{\mathrm{F}}$$

holds as long as $0 < \eta \leq \frac{2}{25\kappa\sigma_{\max}}$, $\rho \geq 1 - \frac{\sigma_{\min}}{4}\eta$, and C_1 is sufficiently large.

Proof. The proof is built upon the restricted strong convexity and smoothness results in Lemma 7. See Appendix B.2. □

Remark 5. This result does not rely on linear convergence w.r.t. the spectral norm.

Further, if the current iterate satisfies (27), then we can derive a stronger sense of error contraction: contraction in terms of the spectral norm.

Lemma 9 (Contraction w.r.t. the spectral norm)*. Suppose that the condition number κ is a constant independent of n. Under the sample complexity that $n^2 p \gg \mu^3 r^3 n \log^3 n$ and the noise condition* (26)*, if the iterates satisfy* (27) *at the tth iteration, then*

$$\left\|\boldsymbol{X}^{t+1}\hat{\boldsymbol{H}}^{t+1} - \boldsymbol{X}^\natural\right\| \leq C_9 \rho^{t+1} \mu r \frac{1}{\sqrt{np}} \left\|\boldsymbol{X}^\natural\right\| + C_{10} \frac{\sigma}{\sigma_{\min}} \sqrt{\frac{n}{p}} \left\|\boldsymbol{X}^\natural\right\| \tag{61}$$

holds with probability at least $1 - O(n^{-10})$, provided that $0 < \eta \leq \frac{1}{2\sigma_{\max}}$ and $\rho \geq 1 - \frac{\sigma_{\min}}{3}\eta$.

Proof. The key observation is this: the iterate that proceeds according to the population-level gradient reduces the error w.r.t. $\|\cdot\|$, namely,

$$\left\| \boldsymbol{X}^t \hat{\boldsymbol{H}}^t - \eta \nabla F\left(\boldsymbol{X}^t \hat{\boldsymbol{H}}^t\right) - \boldsymbol{X}^\natural \right\| < \left\| \boldsymbol{X}^t \hat{\boldsymbol{H}}^t - \boldsymbol{X}^\natural \right\|,$$

as long as $\boldsymbol{X}^t$ is sufficiently close to the truth. Notably, the rotation matrix $\hat{\boldsymbol{H}}^t$ is still chosen to be the one that minimizes the $\|\cdot\|_{\mathrm{F}}$ distance (as opposed to $\|\cdot\|$), which yields a symmetry property $\boldsymbol{X}^{\natural\top} \boldsymbol{X}^t \hat{\boldsymbol{H}}^t = \left(\boldsymbol{X}^t \hat{\boldsymbol{H}}^t\right)^\top \boldsymbol{X}^\natural$ crucial for our analysis. See Appendix B.3 for details. □

7.3 Step 2: introducing leave-one-out sequences and induction hypotheses

7.3.1 Leave-one-out sequences

In order to establish the incoherence properties (27b) for the entire trajectory, we introduce a collection of *leave-one-out* versions of $\{\boldsymbol{X}^t\}_{t\geq 0}$, denoted by $\left\{\boldsymbol{X}^{t,(l)}\right\}_{t\geq 0}$ for each $1 \leq l \leq n$. Specifically, $\left\{\boldsymbol{X}^{t,(l)}\right\}_{t\geq 0}$ is the gradient sequence operating on the auxiliary loss function

$$f^{(l)}(\boldsymbol{X}) := \frac{1}{4p} \left\| \mathcal{P}_{\Omega^{-l}} \left[\boldsymbol{X}\boldsymbol{X}^\top - \left(\boldsymbol{M}^\natural + \boldsymbol{E}\right)\right] \right\|_{\mathrm{F}}^2 + \frac{1}{4} \left\| \mathcal{P}_l \left(\boldsymbol{X}\boldsymbol{X}^\top - \boldsymbol{M}^\natural \right) \right\|_{\mathrm{F}}^2. \tag{62}$$

Here, $\mathcal{P}_{\Omega_l}$ (resp. $\mathcal{P}_{\Omega^{-l}}$ and $\mathcal{P}_l$) represents the orthogonal projection onto the subspace of matrices which vanish outside of the index set $\Omega_l := \{(i,j) \in \Omega \mid i = l \text{ or } j = l\}$ (resp. $\Omega^{-l} := \{(i,j) \in \Omega \mid i \neq l, j \neq l\}$ and $\{(l,j) \cup (j,l) \mid 1 \leq j \leq n\}$); that is, for any matrix $\boldsymbol{M}$,

$$\left[\mathcal{P}_{\Omega_l}(\boldsymbol{M})\right]_{i,j} = \begin{cases} M_{i,j}, & \text{if } (i = l \text{ or } j = l) \text{ and } (i,j) \in \Omega, \\ 0, & \text{else,} \end{cases} \tag{63}$$

$$\left[\mathcal{P}_{\Omega^{-l}}(\boldsymbol{M})\right]_{i,j} = \begin{cases} M_{i,j}, & \text{if } i \neq l \text{ and } j \neq l \text{ and } (i,j) \in \Omega \\ 0, & \text{else} \end{cases} \quad \text{and} \quad \left[\mathcal{P}_l(\boldsymbol{M})\right]_{i,j} = \begin{cases} 0, & \text{if } i \neq l \text{ and } j \neq l, \\ M_{i,j}, & \text{if } i = l \text{ or } j = l. \end{cases} \tag{64}$$

The gradient of the leave-one-out loss function (62) is given by

$$\nabla f^{(l)}(\boldsymbol{X}) = \frac{1}{p} \mathcal{P}_{\Omega^{-l}} \left[\boldsymbol{X}\boldsymbol{X}^\top - \left(\boldsymbol{M}^\natural + \boldsymbol{E}\right)\right] \boldsymbol{X} + \mathcal{P}_l \left(\boldsymbol{X}\boldsymbol{X}^\top - \boldsymbol{M}^\natural \right) \boldsymbol{X}. \tag{65}$$

The whole algorithm to obtain the leave-one-out sequence $\{\boldsymbol{X}^{t,(l)}\}_{t\geq 0}$ (including spectral initialization) is summarized in Algorithm 5.

***Remark* 6.** Rather than simply dropping all samples in the lth row/column, we replace the lth row/column with their respective population means. In other words, the leave-one-out gradient forms an "unbiased" surrogate for the true gradient — this s particularly important in ensuring high estimation accuracy.

Algorithm 5 The lth leave-one-out sequence for matrix completion

Input: $\boldsymbol{Y} = [Y_{i,j}]_{1\leq i,j\leq n}, r, p$.

Spectral initialization: Let $\boldsymbol{U}^{0,(l)} \boldsymbol{\Sigma}^{(l)} \boldsymbol{U}^{0,(l)\top}$ be the top-r eigendecomposition of

$$\boldsymbol{M}^{(l)} := \frac{1}{p} \mathcal{P}_{\Omega^{-l}}(\boldsymbol{Y}) + \mathcal{P}_l\left(\boldsymbol{M}^\natural\right) = \frac{1}{p} \mathcal{P}_{\Omega^{-l}}\left(\boldsymbol{M}^\natural + \boldsymbol{E}\right) + \mathcal{P}_l\left(\boldsymbol{M}^\natural\right)$$

with $\mathcal{P}_{\Omega^{-l}}$ defined in (64), and set $\boldsymbol{X}^{0,(l)} = \boldsymbol{U}^{0,(l)} \left(\boldsymbol{\Sigma}^{(l)}\right)^{1/2}$.

Gradient updates: **for** $t = 0, 1, 2, \ldots, T-1$ **do**

$$\boldsymbol{X}^{t+1,(l)} = \boldsymbol{X}^{t,(l)} - \eta_t \nabla f^{(l)}\left(\boldsymbol{X}^{t,(l)}\right). \tag{66}$$

7.3.2 Induction hypotheses

As we have already seen in Section 7.2.2, the induction hypotheses (27a) and (27c) hold for $t+1$ as long as (27) holds for t. Therefore, we are left with proving the incoherence hypothesis (27b). As usual, we will prove this result in an inductive manner. For clarify of analysis, it is crucial to maintain a list of induction hypotheses, which includes a few hypotheses that complement (27). First-time readers can skip this part and move on to to Section 7.4 directly without losing much continuity.

$$\left\|\boldsymbol{X}^t\hat{\boldsymbol{H}}^t-\boldsymbol{X}^\natural\right\|_\mathrm{F}\le\left(C_4\rho^t\mu r\frac{1}{\sqrt{np}}+C_1\frac{\sigma}{\sigma_{\min}}\sqrt{\frac{n}{p}}\right)\left\|\boldsymbol{X}^\natural\right\|_\mathrm{F}, \tag{67a}$$

$$\left\|\boldsymbol{X}^t\hat{\boldsymbol{H}}^t-\boldsymbol{X}^\natural\right\|_{2,\infty}\le\left(C_5\rho^t\mu r\sqrt{\frac{\log n}{np}}+C_8\frac{\sigma}{\sigma_{\min}}\sqrt{\frac{n\log n}{p}}\right)\left\|\boldsymbol{X}^\natural\right\|_{2,\infty}, \tag{67b}$$

$$\left\|\boldsymbol{X}^t\hat{\boldsymbol{H}}^t-\boldsymbol{X}^\natural\right\|\le\left(C_9\rho^t\mu r\frac{1}{\sqrt{np}}+C_{10}\frac{\sigma}{\sigma_{\min}}\sqrt{\frac{n}{p}}\right)\left\|\boldsymbol{X}^\natural\right\|, \tag{67c}$$

$$\left\|\boldsymbol{X}^t\hat{\boldsymbol{H}}^t-\boldsymbol{X}^{t,(l)}\boldsymbol{R}^{t,(l)}\right\|_\mathrm{F}\le\left(C_3\rho^t\mu r\sqrt{\frac{\log n}{np}}+C_7\frac{\sigma}{\sigma_{\min}}\sqrt{\frac{n\log n}{p}}\right)\left\|\boldsymbol{X}^\natural\right\|_{2,\infty}, \tag{67d}$$

$$\left\|\left(\boldsymbol{X}^{t,(l)}\hat{\boldsymbol{H}}^{t,(l)}-\boldsymbol{X}^\natural\right)_{l,\cdot}\right\|_2\le\left(C_2\rho^t\mu r\frac{1}{\sqrt{np}}+C_6\frac{\sigma}{\sigma_{\min}}\sqrt{\frac{n\log n}{p}}\right)\left\|\boldsymbol{X}^\natural\right\|_{2,\infty} \tag{67e}$$

for some absolute constants $0<\rho<1$ and $C_1,\cdots,C_{10}>0$. Here, $\hat{\boldsymbol{H}}^{t,(l)}$ and $\boldsymbol{R}^{t,(l)}$ are orthonormal matrices defined by

$$\hat{\boldsymbol{H}}^{t,(l)}:=\arg\min_{\boldsymbol{R}\in\mathcal{O}^{r\times r}}\left\|\boldsymbol{X}^{t,(l)}\boldsymbol{R}-\boldsymbol{X}^\natural\right\|_\mathrm{F}, \tag{68}$$

$$\boldsymbol{R}^{t,(l)}:=\arg\min_{\boldsymbol{R}\in\mathcal{O}^{r\times r}}\left\|\boldsymbol{X}^{t,(l)}\boldsymbol{R}-\boldsymbol{X}^t\hat{\boldsymbol{H}}^t\right\|_\mathrm{F}. \tag{69}$$

Clearly, the first three hypotheses (67a)-(67c) constitute the conclusion of Theorem (2). The last two hypotheses (67d) and (67e) are auxiliary properties connecting the true iterates and the auxiliary sequence, which we will explain later.

Moreover, we summarize below several immediate consequences of (67), which will be useful throughout.

***Lemma* 10.** *Suppose the sample complexity obeys $n\gg\kappa^3\mu r\log n$. Under the hypotheses* (67)*, one has*

$$\left\|\boldsymbol{X}^{t,(l)}\hat{\boldsymbol{H}}^{t,(l)}-\boldsymbol{X}^\natural\right\|_\mathrm{F}\le\left\|\boldsymbol{X}^{t,(l)}\boldsymbol{R}^{t,(l)}-\boldsymbol{X}^\natural\right\|_\mathrm{F}\le\left\{2C_4\rho^t\mu r\frac{1}{\sqrt{np}}+2C_1\frac{\sigma}{\sigma_{\min}}\sqrt{\frac{n}{p}}\right\}\left\|\boldsymbol{X}^\natural\right\|_\mathrm{F}, \tag{70a}$$

$$\left\|\boldsymbol{X}^{t,(l)}\boldsymbol{R}^{t,(l)}-\boldsymbol{X}^\natural\right\|_{2,\infty}\le\left\{\left(C_3+C_5\right)\rho^t\mu r\sqrt{\frac{\log n}{np}}+\left(C_8+C_7\right)\frac{\sigma}{\sigma_{\min}}\sqrt{\frac{n\log n}{p}}\right\}\left\|\boldsymbol{X}^\natural\right\|_{2,\infty}, \tag{70b}$$

$$\left\|\boldsymbol{X}^{t,(l)}\hat{\boldsymbol{H}}^{t,(l)}-\boldsymbol{X}^\natural\right\|\le\left\{2C_9\rho^t\mu r\frac{1}{\sqrt{np}}+2C_{10}\frac{\sigma}{\sigma_{\min}}\sqrt{\frac{n}{p}}\right\}\left\|\boldsymbol{X}^\natural\right\|. \tag{70c}$$

Proof. See Appendix B.4. □

7.4 Step 3: establishing the incoherence condition (27b)

The main objective of this section is to establish the incoherence property (27b) (or (67b)) for all $0\le t\le T=O(n^5)$, which is difficult to deal with directly due to complicated statistical dependency. As suggested by the general recipe, we resort to the leave-one-out iterates by showing that (1) the true and the auxiliary iterates remain exceedingly close throughout; (2) the lth leave-one-out sequence stays incoherent with $\boldsymbol{e}_l$ due to statistical independence. We follow the three steps outlined in the general recipe.

- **Step 3(a): proximity between the original and the leave-one-out iterates.** We demonstrate that $\boldsymbol{X}^{t+1}$ is very well approximated by $\boldsymbol{X}^{t+1,(l)}$ (up to proper rotation). This is precisely the hypothesis (67d) for $t+1$.

  ***Lemma* 11.** *Suppose the sample complexity satisfies $n^2p \gg \kappa^4\mu^3r^3n\log^3 n$ and the noise satisfies* (26)*. Under the hypotheses* (67) *for the tth iteration, we have*

  $$\left\| \boldsymbol{X}^{t+1}\hat{\boldsymbol{H}}^{t+1} - \boldsymbol{X}^{t+1,(l)}\boldsymbol{R}^{t+1,(l)} \right\|_{\mathrm{F}} \leq C_3\rho^{t+1}\mu r\sqrt{\frac{\log n}{np}}\left\|\boldsymbol{X}^\natural\right\|_{2,\infty} + C_7\frac{\sigma}{\sigma_{\min}}\sqrt{\frac{n\log n}{p}}\left\|\boldsymbol{X}^\natural\right\|_{2,\infty} \tag{71}$$

  with probability at least $1-O(n^{-10})$, provided that $0<\eta\leq\frac{2}{25\kappa\sigma_{\max}}$ and $\rho\geq 1-\frac{\sigma_{\min}}{5}\eta$.

  Proof. The fact that this difference does not blow up relies heavily on the restricted strong convexity and smoothness revealed by Lemma 7. Two important remarks are in order: (1) both points $\boldsymbol{X}^t\hat{\boldsymbol{H}}^t$ and $\boldsymbol{X}^{t,(l)}\boldsymbol{R}^{t,(l)}$ satisfy the first condition (the one specified for $\boldsymbol{X}$) required therein; (2) the difference $\boldsymbol{X}^t\hat{\boldsymbol{H}}^t - \boldsymbol{X}^{t,(l)}\boldsymbol{R}^{t,(l)}$ forms a valid direction for restricted strong convexity (namely, it satisfies the condition for $\boldsymbol{V}$). These two properties allow us to invoke Lemma 7. See Appendix B.5. ☐

- **Step 3(b): incoherence of the leave-one-out iterates.** Given that $\boldsymbol{X}^{t+1,(l)}$ is sufficiently close to $\boldsymbol{X}^{t+1}$, we turn attention to showing the incoherence of this surrogate $\boldsymbol{X}^{t+1,(l)}$ w.r.t. $\boldsymbol{e}_l$. This amounts to proving the hypothesis (67e) for $t+1$.

  ***Lemma* 12.** *Suppose the sample complexity meets $n^2p \gg \kappa^3\mu^3r^3n\log^3 n$ and the noise satisfies* (26)*. Under the hypotheses* (67) *for the tth iteration, one has*

  $$\left\| \left(\boldsymbol{X}^{t+1,(l)}\hat{\boldsymbol{H}}^{t+1,(l)} - \boldsymbol{X}^\natural\right)_{l,\cdot} \right\|_2 \leq C_2\rho^{t+1}\mu r\frac{1}{\sqrt{np}}\left\|\boldsymbol{X}^\natural\right\|_{2,\infty} + C_6\frac{\sigma}{\sigma_{\min}}\sqrt{\frac{n\log n}{p}}\left\|\boldsymbol{X}^\natural\right\|_{2,\infty} \tag{72}$$

  with probability at least $1-O(n^{-10})$, as long as $0<\eta\leq\frac{1}{\sigma_{\max}}$, $\rho\geq 1-\frac{\sigma_{\min}}{3}\eta$, $C_2\gg\kappa C_9$ and $C_6\gg\kappa C_{10}$.

  Proof. The key observation is that $\boldsymbol{X}^{t+1,(l)}$ is statistically independent from any sample in the lth row/column of the matrix. Since there are an order of np samples in each row/column, we obtain enough information that helps establish the desired incoherence property. See Appendix B.6. ☐

- **Step 3(c): combining the bounds.** The inequalities (67e) and (67d) taken collectively allow us to establish (67b). Specifically, for every $1\leq l\leq n$, write

  $$\left(\boldsymbol{X}^{t+1}\hat{\boldsymbol{H}}^{t+1} - \boldsymbol{X}^\natural\right)_{l,\cdot} = \left(\boldsymbol{X}^{t+1}\hat{\boldsymbol{H}}^{t+1} - \boldsymbol{X}^{t+1,(l)}\hat{\boldsymbol{H}}^{t+1,(l)}\right)_{l,\cdot} + \left(\boldsymbol{X}^{t+1,(l)}\hat{\boldsymbol{H}}^{t+1,(l)} - \boldsymbol{X}^\natural\right)_{l,\cdot},$$

  and the triangle inequality gives

  $$\left\|\left(\boldsymbol{X}^{t+1}\hat{\boldsymbol{H}}^{t+1} - \boldsymbol{X}^\natural\right)_{l,\cdot}\right\|_2 \leq \left\|\boldsymbol{X}^{t+1}\hat{\boldsymbol{H}}^{t+1} - \boldsymbol{X}^{t+1,(l)}\hat{\boldsymbol{H}}^{t+1,(l)}\right\|_{\mathrm{F}} + \left\|\left(\boldsymbol{X}^{t+1,(l)}\hat{\boldsymbol{H}}^{t+1,(l)} - \boldsymbol{X}^\natural\right)_{l,\cdot}\right\|_2. \tag{73}$$

  The second term has already been bounded by (67e). The first term is quite similar to the term studied in Lemma 11, except that the rotation matrix is different. We expect to obtain some stability guarantee and claim that

  $$\left\|\boldsymbol{X}^t\hat{\boldsymbol{H}}^t - \boldsymbol{X}^{t,(l)}\hat{\boldsymbol{H}}^{t,(l)}\right\|_{\mathrm{F}} \leq 5\kappa\left\|\boldsymbol{X}^t\hat{\boldsymbol{H}}^t - \boldsymbol{X}^{t,(l)}\boldsymbol{R}^{t,(l)}\right\|_{\mathrm{F}}. \tag{74}$$

  Plugging (74) and (67e) into (73), we have

  $$\begin{aligned}\left\|\boldsymbol{X}^t\hat{\boldsymbol{H}}^t - \boldsymbol{X}^\natural\right\|_{2,\infty} \leq 5\kappa&\left(C_3\rho^t\mu r\sqrt{\frac{\log n}{np}}\left\|\boldsymbol{X}^\natural\right\|_{2,\infty} + \frac{C_7}{\sigma_{\min}}\sigma\sqrt{\frac{n\log n}{p}}\left\|\boldsymbol{X}^\natural\right\|_{2,\infty}\right)\\ &+ C_2\rho^t\mu r\frac{1}{\sqrt{np}}\left\|\boldsymbol{X}^\natural\right\|_{2,\infty} + \frac{C_6}{\sigma_{\min}}\sigma\sqrt{\frac{n\log n}{p}}\left\|\boldsymbol{X}^\natural\right\|_{2,\infty}\end{aligned}$$

$$\leq C_5\rho^t\mu r\sqrt{\frac{\log n}{np}}\left\|\boldsymbol{X}^\natural\right\|_{2,\infty}+\frac{C_8}{\sigma_{\min}}\sigma\sqrt{\frac{n\log n}{p}}\left\|\boldsymbol{X}^\natural\right\|_{2,\infty}$$

as long as $C_5/(\kappa C_3 + C_2)$ is sufficiently large. This finishes the proof.

Proof of the claim (74). Letting $\boldsymbol{X}_1 = \boldsymbol{X}^t\hat{\boldsymbol{H}}^t$ and $\boldsymbol{X}_2 = \boldsymbol{X}^{t,(l)}\boldsymbol{R}^{t,(l)}$ as in Lemma 41, we get

$$\left\|\boldsymbol{X}_1-\boldsymbol{X}^\natural\right\|\left\|\boldsymbol{X}^\natural\right\| \overset{\text{(i)}}{\leq} C_9\rho^t\mu r\frac{1}{\sqrt{np}}\sigma_{\max}+\frac{C_{10}}{\sigma_{\min}}\sigma\sqrt{\frac{n\log n}{p}}\sigma_{\max} \overset{\text{(ii)}}{\leq} \frac{1}{2}\sigma_{\min},$$

where (i) follows from (67c) and (ii) holds as long as $n^2p \gg \kappa^2\mu^2r^2n$. In addition,

$$\begin{aligned}
\left\|\boldsymbol{X}_1-\boldsymbol{X}_2\right\|\left\|\boldsymbol{X}^\natural\right\| &\leq \left\|\boldsymbol{X}_1-\boldsymbol{X}_2\right\|_{\mathrm{F}}\left\|\boldsymbol{X}^\natural\right\| \\
&\overset{\text{(i)}}{\leq} \left(C_3\rho^t\mu r\sqrt{\frac{\log n}{np}}\left\|\boldsymbol{X}^\natural\right\|_{2,\infty}+\frac{C_7}{\sigma_{\min}}\sigma\sqrt{\frac{n\log n}{p}}\left\|\boldsymbol{X}^\natural\right\|_{2,\infty}\right)\left\|\boldsymbol{X}^\natural\right\| \\
&\overset{\text{(ii)}}{\leq} C_3\rho^t\mu r\sqrt{\frac{\log n}{np}}\sigma_{\max}+\frac{C_7}{\sigma_{\min}}\sigma\sqrt{\frac{n\log n}{p}}\sigma_{\max} \\
&\overset{\text{(iii)}}{\leq} \sigma_{\min}/2,
\end{aligned}$$

where (i) utilizes (67d), (ii) follows since $\left\|\boldsymbol{X}^\natural\right\|_{2,\infty} \leq \left\|\boldsymbol{X}^\natural\right\|$, and (iii) holds if $n^2p \gg \kappa^2\mu^2r^2n\log n$ and $\sigma\sqrt{\frac{n\log n}{p}} \ll \sigma_{\min}$. With these in place, Lemma 41 immediately yields (74). □

7.5 The base case

Finally, we return to check the base case, namely, we aim to show that the spectral initialization satisfies the induction hypotheses (67a)-(67e). This is accomplished via the following lemma.

Lemma 13. *Suppose the sample size obeys $n^2p \gg \mu^2r^2n\log n$ and the noise satisfies (26). Then with probability at least $1-O\left(n^{-10}\right)$,* (67a)-(67e) *hold simultaneously.*

Proof. This follows by invoking the Davis-Kahan $\sin\Theta$ theorem [DK70] as well as the entrywise eigenvector perturbation analysis in [AFWZ17]. We defer the proof to Appendix B.7. □

8 Analysis for blind deconvolution

This section is devoted to the analysis of the vanilla gradient descent algorithm for the blind deconvolution problem (i.e. Theorem 3). Without loss of generality, we assume throughout that $\left\|\boldsymbol{h}^\natural\right\|_2 = \left\|\boldsymbol{x}^\natural\right\|_2 = 1$. Before presenting the full analysis, we first gather some simple facts about the loss function in (31).

8.1 Preliminaries and notations

Throughout this section, for any matrix $\boldsymbol{A} \in \mathbb{C}^{n_1\times n_2}$, we denote by $\boldsymbol{A}^\top \in \mathbb{C}^{n_2\times n_1}$ the transpose of $\boldsymbol{A}$, $\boldsymbol{A}^* \in \mathbb{C}^{n_2\times n_1}$ the conjugate transpose of $\boldsymbol{A}$, and $\overline{\boldsymbol{A}} \in \mathbb{C}^{n_1\times n_2}$ the entrywise conjugate of $\boldsymbol{A}$. Also, we use $\mathrm{Re}(x)$ to denote the real part of a complex number x. The Wirtinger gradient of (31) with respect to $\boldsymbol{h}$ and $\boldsymbol{x}$ are given respectively by

$$\nabla_{\boldsymbol{h}}f\left(\boldsymbol{h},\boldsymbol{x}\right) = \sum_{j=1}^{m}\left(\boldsymbol{b}_j^*\boldsymbol{h}\boldsymbol{x}^*\boldsymbol{a}_j - y_j\right)\boldsymbol{b}_j\boldsymbol{a}_j^*\boldsymbol{x}; \tag{75}$$

$$\nabla_{\boldsymbol{x}}f\left(\boldsymbol{h},\boldsymbol{x}\right) = \sum_{j=1}^{m}\overline{\left(\boldsymbol{b}_j^*\boldsymbol{h}\boldsymbol{x}^*\boldsymbol{a}_j - y_j\right)}\boldsymbol{a}_j\boldsymbol{b}_j^*\boldsymbol{h}. \tag{76}$$

It is worth noting that the formal Wirtinger gradient contains $\nabla_{\overline{\boldsymbol{h}}} f(\boldsymbol{h}, \boldsymbol{x})$ and $\nabla_{\overline{\boldsymbol{x}}} f(\boldsymbol{h}, \boldsymbol{x})$ as well. Since $f(\boldsymbol{h}, \boldsymbol{x})$ is a real-valued function, the following identities always hold

$$\nabla_{\boldsymbol{h}} f(\boldsymbol{h}, \boldsymbol{x}) = \overline{\nabla_{\overline{\boldsymbol{h}}} f(\boldsymbol{h}, \boldsymbol{x})} \qquad \text{and} \qquad \nabla_{\boldsymbol{x}} f(\boldsymbol{h}, \boldsymbol{x}) = \overline{\nabla_{\overline{\boldsymbol{x}}} f(\boldsymbol{h}, \boldsymbol{x})}.$$

In light of these observations, one often omit the gradient with respect to the conjugates; see [CLS15, Section 6] for relevant discussion. Correspondingly, the gradient update rules can be written as

$$\boldsymbol{h}^{t+1} = \boldsymbol{h}^t - \frac{\eta}{\|\boldsymbol{x}^t\|_2^2} \sum_{j=1}^{m} \left(\boldsymbol{b}_j^* \boldsymbol{h}^t \boldsymbol{x}^{t*} \boldsymbol{a}_j - y_j\right) \boldsymbol{b}_j \boldsymbol{a}_j^* \boldsymbol{x}^t, \tag{77}$$

$$\boldsymbol{x}^{t+1} = \boldsymbol{x}^t - \frac{\eta}{\|\boldsymbol{h}^t\|_2^2} \sum_{j=1}^{m} \overline{(\boldsymbol{b}_j^* \boldsymbol{h}^t \boldsymbol{x}^{t*} \boldsymbol{a}_j - y_j)} \boldsymbol{a}_j \boldsymbol{b}_j^* \boldsymbol{h}^t. \tag{78}$$

We can also compute the Wirtinger Hessian of $f(\cdot)$ as follows (see [CLS15, Section 6] for the definition of Wirtinger Hessian)

$$\nabla^2 f(\boldsymbol{z}) = \begin{bmatrix} \boldsymbol{A} & \boldsymbol{B} \\ \boldsymbol{B}^* & \overline{\boldsymbol{A}} \end{bmatrix}, \tag{79}$$

where

$$\boldsymbol{A} = \begin{bmatrix} \sum_{j=1}^m \left|\boldsymbol{a}_j^* \boldsymbol{x}\right|^2 \boldsymbol{b}_j \boldsymbol{b}_j^* & \sum_{j=1}^m \left(\boldsymbol{b}_j^* \boldsymbol{h} \boldsymbol{x}^* \boldsymbol{a}_j - y_j\right) \boldsymbol{b}_j \boldsymbol{a}_j^* \\ \sum_{j=1}^m \left[\left(\boldsymbol{b}_j^* \boldsymbol{h} \boldsymbol{x}^* \boldsymbol{a}_j - y_j\right) \boldsymbol{b}_j \boldsymbol{a}_j^*\right]^* & \sum_{j=1}^m \left|\boldsymbol{b}_j^* \boldsymbol{h}\right|^2 \boldsymbol{a}_j \boldsymbol{a}_j^* \end{bmatrix} \in \mathbb{C}^{2K \times 2K};$$

$$\boldsymbol{B} = \begin{bmatrix} \boldsymbol{0} & \sum_{j=1}^m \boldsymbol{b}_j \boldsymbol{b}_j^* \boldsymbol{h} \left(\boldsymbol{a}_j \boldsymbol{a}_j^* \boldsymbol{x}\right)^\top \\ \sum_{j=1}^m \boldsymbol{a}_j \boldsymbol{a}_j^* \boldsymbol{x} \left(\boldsymbol{b}_j \boldsymbol{b}_j^* \boldsymbol{h}\right)^\top & \boldsymbol{0} \end{bmatrix} \in \mathbb{C}^{2K \times 2K}.$$

For notational simplicity, we write $f(\boldsymbol{z}) = f(\boldsymbol{h}, \boldsymbol{x})$, and define

$$\tilde{\boldsymbol{h}}^t := \frac{1}{\overline{\alpha^t}} \boldsymbol{h}^t \qquad \text{and} \qquad \tilde{\boldsymbol{x}}^t := \alpha^t \boldsymbol{x}^t \tag{80}$$

with $\alpha^t := \arg\min_{\alpha \in \mathbb{C}} \left\| \frac{1}{\overline{\alpha}} \boldsymbol{h}^t - \boldsymbol{h}^\natural \right\|_2^2 + \left\| \alpha \boldsymbol{x}^t - \boldsymbol{x}^\natural \right\|_2^2$ as usual. This gives

$$\operatorname{dist}\left(\boldsymbol{z}^t, \boldsymbol{z}^\natural\right) = \left\| \begin{bmatrix} \tilde{\boldsymbol{h}}^t - \boldsymbol{h}^\natural \\ \tilde{\boldsymbol{x}}^t - \boldsymbol{x}^\natural \end{bmatrix} \right\|_2.$$

8.2 Step 1: characterizing local geometry in the RIC

8.2.1 Local geometry

Recall from the general recipe that the first step we need to achieve is to characterize the region of incoherence and contraction (RIC). To this end, we have the following lemma.

***Lemma* 14.** *[Restricted strong convexity and smoothness for blind deconvolution]Let $\delta > 0$ be some sufficiently small constant. Suppose the sample size satisfies $m \gg \mu^2 K \log^5 m$. Then with probability at least $1 - O\left(m^{-10}\right)$, the Wirtinger Hessian $\nabla^2 f(\boldsymbol{z})$ obeys*

$$\boldsymbol{u}^* \left[\boldsymbol{D} \nabla^2 f(\boldsymbol{z}) + \nabla^2 f(\boldsymbol{z}) \boldsymbol{D}\right] \boldsymbol{u} \geq \frac{1}{4} \|\boldsymbol{u}\|_2^2 \qquad \textit{and} \qquad \left\|\nabla^2 f(\boldsymbol{z})\right\| \leq 3$$

simultaneously for all

$$\boldsymbol{z} = \begin{bmatrix} \boldsymbol{h} \\ \boldsymbol{x} \end{bmatrix} \qquad \textit{and} \qquad \boldsymbol{u} = \begin{bmatrix} \boldsymbol{h}_1 - \boldsymbol{h}_2 \\ \boldsymbol{x}_1 - \boldsymbol{x}_2 \\ \overline{\boldsymbol{h}_1 - \boldsymbol{h}_2} \\ \overline{\boldsymbol{x}_1 - \boldsymbol{x}_2} \end{bmatrix} \qquad \textit{and} \qquad \boldsymbol{D} = \begin{bmatrix} \gamma_1 \boldsymbol{I}_K & & & \\ & \gamma_2 \boldsymbol{I}_K & & \\ & & \gamma_1 \boldsymbol{I}_K & \\ & & & \gamma_2 \boldsymbol{I}_K \end{bmatrix}$$

satisfying the following conditions:

- $\max\left\{\left\|\boldsymbol{h}-\boldsymbol{h}^{\natural}\right\|_2, \left\|\boldsymbol{x}-\boldsymbol{x}^{\natural}\right\|_2\right\} \le \delta$;
- $\max_{1\le j\le m}\left|\boldsymbol{a}_j^*\left(\boldsymbol{x}-\boldsymbol{x}^{\natural}\right)\right| \le 2C_3\frac{1}{\log^{3/2} m}$ *and* $\max_{1\le j\le m}\left|\boldsymbol{b}_j^*\boldsymbol{h}\right| \le 2C_4\frac{\mu}{\sqrt{m}}\log^2 m$;
- $\max\left\{\left\|\boldsymbol{h}_1-\boldsymbol{h}^{\natural}\right\|_2, \left\|\boldsymbol{h}_2-\boldsymbol{h}^{\natural}\right\|_2, \left\|\boldsymbol{x}_1-\boldsymbol{x}^{\natural}\right\|_2, \left\|\boldsymbol{x}_2-\boldsymbol{x}^{\natural}\right\|_2\right\} \le \delta$;
- $(\boldsymbol{h}_1, \boldsymbol{x}_1)$ *is aligned with* $(\boldsymbol{h}_2, \boldsymbol{x}_2)$*, namely,*

$$\left\|\boldsymbol{h}_1-\boldsymbol{h}_2\right\|_2^2+\left\|\boldsymbol{x}_1-\boldsymbol{x}_2\right\|_2^2=\min_{\alpha\in\mathbb{C}}\left\{\left\|\frac{1}{\overline{\alpha}}\boldsymbol{h}_1-\boldsymbol{h}_2\right\|_2^2+\left\|\alpha\boldsymbol{x}_1-\boldsymbol{x}_2\right\|_2^2\right\};$$

- $\gamma_1, \gamma_2 \in \mathbb{R}$ *and* $\max\left\{\left|\gamma_1-1\right|, \left|\gamma_2-1\right|\right\} \le \delta$.

Here, $C_3, C_4 > 0$ *are numerical constants.*

Proof. See Appendix C.1. □

Lemma 14 characterizes the restricted strong convexity and smoothness of the loss function. A few interpretations are in order.

- The first two conditions specify the region of incoherence and contraction (RIC).
- As in the matrix completion case, the Hessian matrix is rank-deficient even in the population level. Consequently, we resort to a restricted form of strong convexity by restricting attention to certain directions. More specifically, these directions can be viewed as the difference between two points that are not far from the truth and that are pre-aligned.
- Including the scaling matrix $\boldsymbol{D}$ allows us to account for different step sizes employed for $\boldsymbol{h}$ and $\boldsymbol{x}$.

To the best of our knowledge, this provides the first characterization regarding the strong convexity of the Hessian matrix for blind deconvolution.

8.2.2 Error contraction

The restricted strong convexity and smoothness allow us to establish contraction of the error measured by the dist metric as defined in (32).

***Lemma* 15.** *Suppose the number of measurements satisfies* $m \gg \mu^2 K \log^5 m$*, and the step size* $\eta > 0$ *is some sufficiently small constant. Then with probability exceeding* $1-O(m^{-10})$*,*

$$\operatorname{dist}\left(\boldsymbol{z}^{t+1}, \boldsymbol{z}^{\natural}\right) \le (1-\eta/16)\operatorname{dist}\left(\boldsymbol{z}^{t}, \boldsymbol{z}^{\natural}\right),$$

provided that

$$\operatorname{dist}\left(\boldsymbol{z}^{t}, \boldsymbol{z}^{\natural}\right) \le \xi, \tag{81a}$$

$$\max_{1\le j\le m}\left|\boldsymbol{a}_j^*\left(\tilde{\boldsymbol{x}}^t-\boldsymbol{x}^{\natural}\right)\right| \le C_3\frac{1}{\log^{1.5} m}, \tag{81b}$$

$$\max_{1\le j\le m}\left|\boldsymbol{b}_j^*\tilde{\boldsymbol{h}}^t\right| \le C_4\frac{\mu}{\sqrt{m}}\log^2 m. \tag{81c}$$

for some constants $C_3, C_4 > 0$*. Here,* $\tilde{\boldsymbol{h}}^t$ *and* $\tilde{\boldsymbol{x}}^t$ *are defined in (80), and* $\xi > 0$ *is some sufficiently small constant.*

Proof. See Appendix C.2. □

As a result, if $\boldsymbol{z}^t$ satisfies the condition (81) for all $0 \le t \le T = O(m^5)$, then the union bound gives

$$\operatorname{dist}\left(\boldsymbol{z}^{t}, \boldsymbol{z}^{\natural}\right) \le \rho\operatorname{dist}\left(\boldsymbol{z}^{t-1}, \boldsymbol{z}^{\natural}\right) \le \rho^t\operatorname{dist}\left(\boldsymbol{z}^{0}, \boldsymbol{z}^{\natural}\right) \le \rho^t c_1, \qquad 0 < t \le T$$

with probability exceeding $1-O(m^{-5})$.

Furthermore, as in phase retrieval (i.e. Lemma 3), we can show that as long as the condition (81) holds for all $0 \le t \le m$, then Theorem 3 holds true. The proof of this claim is exactly the same as for Lemma 3, and is thus omitted for conciseness. In what follows, we focus on establishing (81) for all $0 \le t \le m$.

8.3 Step 2: introducing leave-one-out sequences and induction hypotheses

8.3.1 Leave-one-out sequences

As demonstrated by the assumptions in Lemma 15, the key is to show that the whole trajectory lies in the region specified by (81a)-(81c). Once again, the difficulty lies in the statistical dependency between the iterates $\{z^t\}$ and the measurement vectors $\{a_j\}$. We follow the general recipe and introduce the *leave-one-out* sequences, denoted by $\{h^{t,(l)}, x^{t,(l)}\}_{t\geq 0}$ for each $1 \leq l \leq m$. Specifically, $\{h^{t,(l)}, x^{t,(l)}\}_{t\geq 0}$ is the gradient sequence operating on the loss function

$$f^{(l)}(h, x) := \sum_{j:j\neq l} \left| b_j^* \left(h x^* - h^\natural x^{\natural *} \right) a_j \right|^2 . \tag{82}$$

Then whole sequence is constructed by a spectral method followed by vanilla GD on the leave-one-out loss (82). The precise description is supplied in Algorithm 6.

For notational simplicity, we will set $z^{t,(l)} = \begin{bmatrix} h^{t,(l)} \\ x^{t,(l)} \end{bmatrix}$ and $f(z^{t,(l)}) = f(h^{t,(l)}, x^{t,(l)})$, define

$$\alpha^{t,(l)} := \arg\min_{\alpha\in\mathbb{C}} \left\| \frac{1}{\overline{\alpha}} h^{t,(l)} - h^\natural \right\|_2^2 + \left\| \alpha x^{t,(l)} - x^\natural \right\|_2^2, \tag{83}$$

and denote

$$\tilde{h}^{t,(l)} = \frac{1}{\overline{\alpha^{t,(l)}}} h^{t,(l)} \qquad \text{and} \qquad \tilde{x}^{t,(l)} = \alpha^{t,(l)} x^{t,(l)}. \tag{84}$$

Algorithm 6 The lth leave-one-out sequence for blind deconvolution

Input: $\{a_j\}_{1\leq j\leq m, j\neq l}$, $\{b_j\}_{1\leq j\leq m, j\neq l}$ and $\{y_j\}_{1\leq j\leq m, j\neq l}$.

Spectral initialization: Set $\sigma_1(M^{(l)})$, $\check{h}^{0,(l)}$ and $\check{x}^{0,(l)}$ to be the leading singular value, left and right singular vectors of

$$M^{(l)} := \sum_{j:j\neq l} y_j b_j a_j^*,$$

respectively. Let $h^{0,(l)} = \sqrt{\sigma_1(M^{(l)})}\, \check{h}^{0,(l)}$ and $x^{0,(l)} = \sqrt{\sigma_1(M^{(l)})}\, \check{x}^{0,(l)}$.

Gradient updates: **for** $t = 0, 1, 2, \dots, T-1$ **do**

$$\begin{bmatrix} h^{t+1,(l)} \\ x^{t+1,(l)} \end{bmatrix} = \begin{bmatrix} h^{t,(l)} \\ x^{t,(l)} \end{bmatrix} - \eta \begin{bmatrix} \frac{1}{\|x^{t,(l)}\|_2^2} \nabla_h f^{(l)}\big(h^{t,(l)}, x^{t,(l)}\big) \\ \frac{1}{\|h^{t,(l)}\|_2^2} \nabla_x f^{(l)}\big(h^{t,(l)}, x^{t,(l)}\big) \end{bmatrix}. \tag{85}$$

8.3.2 Induction hypotheses

As usual, the proof is built upon the nice properties of the leave-one-out sequences, and follows an inductive argument. For clarity of presentation, we list below the set of induction hypotheses underlying our analysis. First-time readers can skip directly to the next step.

$$\mathrm{dist}\left(z^t, z^\natural\right) \leq C_1 \frac{1}{\log^2 m}, \tag{86a}$$

$$\mathrm{dist}\big(z^{t,(l)}, \tilde{z}^t\big) \leq C_2 \frac{\mu}{\sqrt{m}} \sqrt{\frac{\mu^2 K \log^9 m}{m}}, \tag{86b}$$

$$\max_{1\leq l\leq m} \left| a_l^* \big(\tilde{x}^t - x^\natural\big) \right| \leq C_3 \frac{1}{\log^{1.5} m}, \tag{86c}$$

$$\max_{1\leq l\leq m} \left| b_l^* \tilde{h}^t \right| \leq C_4 \frac{\mu}{\sqrt{m}} \log^2 m. \tag{86d}$$

where $\tilde{\boldsymbol{h}}^t$ and $\tilde{\boldsymbol{x}}^t$ are defined in (80). Here, $C_1, C_3 > 0$ are some sufficiently small constants, while $C_2, C_4 > 0$ are some sufficiently large constants. We aim to show that if these hypotheses hold in the tth iteration, then the same would hold for $t+1$.

The first hypothesis regarding $\mathrm{dist}(\boldsymbol{z}^t, \boldsymbol{z}^\natural)$ has already been established in Lemma 15, and hence the rest of this section focuses on establishing the remaining three.

8.4 Step 3: establishing the incoherence condition

In this subsection, we assume that (86) holds for the tth iteration, and then justify the incoherence hypotheses (86d) and (86c) for $t+1$. Towards this, we also need to establish (86b) for $t+1$. In the sequel, we follow the steps suggested in the general recipe.

- **Step 3(a): proximity between the original and the leave-one-out iterates.** We first justify the hypothesis (86b) for $t+1$ via the following lemma.

  ***Lemma* 16.** *Suppose the sample complexity obeys $m \gg \mu^2 K \log^6 m$. Under the hypotheses (86a)-(86d) for the tth iteration, one has*

$$\mathrm{dist}\big(\boldsymbol{z}^{t+1,(l)}, \tilde{\boldsymbol{z}}^{t+1}\big) \le C_2 \frac{\mu}{\sqrt{m}} \sqrt{\frac{\mu^2 K \log^9 m}{m}}$$

$$\text{and} \qquad \max_{1\le l\le m} \big\|\tilde{\boldsymbol{z}}^{t+1,(l)} - \tilde{\boldsymbol{z}}^{t+1}\big\|_2 \lesssim C_2 \frac{\mu}{\sqrt{m}} \sqrt{\frac{\mu^2 K \log^9 m}{m}},$$

  with probability at least $1 - O\left(m^{-10}\right)$, provided the step size $\eta > 0$ is some sufficiently small constant.

  Proof. As usual, this result follows from restricted strong convexity, which forces the distance between the two sequences of interest to be contractive. See Appendix C.3. □

- **Step 3(b): incoherence of the leave-one-out iterate $\boldsymbol{x}^{t+1,(l)}$ w.r.t. $\boldsymbol{a}_l$.** Next, we show that the leave-one iterate $\tilde{\boldsymbol{x}}^{t+1,(l)}$ — which is independent from $\boldsymbol{a}_l$ — is incoherent w.r.t. $\boldsymbol{a}_l$ in the sense that

$$\left|\boldsymbol{a}_l^* \big(\tilde{\boldsymbol{x}}^{t+1,(l)} - \boldsymbol{x}^\natural\big)\right| \le 10 C_1 \frac{1}{\log^{3/2} m} \tag{87}$$

  with probability exceeding $1 - O\left(m^{-10}\right)$. To see why, use the statistical independence and the standard Gaussian concentration inequality to show that

$$\max_{1\le l\le m} \left|\boldsymbol{a}_l^* \big(\tilde{\boldsymbol{x}}^{t+1,(l)} - \boldsymbol{x}^\natural\big)\right| \le 5\sqrt{\log m} \max_{1\le l\le m} \big\|\tilde{\boldsymbol{x}}^{t+1,(l)} - \boldsymbol{x}^\natural\big\|_2$$

  with probability exceeding $1 - O(m^{-10})$. It then follows from the triangle inequality that

$$\begin{aligned} \big\|\tilde{\boldsymbol{x}}^{t+1,(l)} - \boldsymbol{x}^\natural\big\|_2 &\le \big\|\tilde{\boldsymbol{x}}^{t+1,(l)} - \tilde{\boldsymbol{x}}^{t+1}\big\|_2 + \big\|\tilde{\boldsymbol{x}}^{t+1} - \boldsymbol{x}^\natural\big\|_2 \\ &\overset{\text{(i)}}{\le} C \frac{\mu}{\sqrt{m}} \sqrt{\frac{\mu^2 K \log^9 m}{m}} + C_1 \frac{1}{\log^2 m} \\ &\overset{\text{(ii)}}{\le} 2 C_1 \frac{1}{\log^2 m}, \end{aligned}$$

  where (i) follows from Lemmas 15 and 16, and (ii) holds as soon as $m \gg \mu^2 \sqrt{K} \log^{13/2} m$. Combining the preceding two bounds establishes (87).

- **Step 3(c): combining the bounds to show incoherence of $\boldsymbol{x}^{t+1}$ w.r.t. $\{\boldsymbol{a}_l\}$.** The above bounds immediately allow us to conclude that

$$\max_{1\le l\le m} \left|\boldsymbol{a}_l^* \big(\tilde{\boldsymbol{x}}^{t+1} - \boldsymbol{x}^\natural\big)\right| \le C_3 \frac{1}{\log^{3/2} m}$$

with probability at least $1-O\left(m^{-10}\right)$, which is exactly the hypothesis (86c) for $t+1$. Specifically, for each $1\le l\le m$, the triangle inequality yields

$$\begin{aligned}\left|\boldsymbol{a}_l^*\left(\tilde{\boldsymbol{x}}^{t+1}-\boldsymbol{x}^\natural\right)\right| &\le \left|\boldsymbol{a}_l^*\left(\tilde{\boldsymbol{x}}^{t+1}-\tilde{\boldsymbol{x}}^{t+1,(l)}\right)\right|+\left|\boldsymbol{a}_l^*\left(\tilde{\boldsymbol{x}}^{t+1,(l)}-\boldsymbol{x}^\natural\right)\right| \\ &\overset{\text{(i)}}{\le} \|\boldsymbol{a}_l\|_2\left\|\tilde{\boldsymbol{x}}^{t+1}-\tilde{\boldsymbol{x}}^{t+1,(l)}\right\|_2+\left|\boldsymbol{a}_l^*\left(\tilde{\boldsymbol{x}}^{t+1,(l)}-\boldsymbol{x}^\natural\right)\right| \\ &\overset{\text{(ii)}}{\le} 3\sqrt{K}\cdot C\frac{\mu}{\sqrt{m}}\sqrt{\frac{\mu^2K\log^9 m}{m}}+10C_1\frac{1}{\log^{3/2}m} \\ &\overset{\text{(iii)}}{\le} C_3\frac{1}{\log^{3/2}m}.\end{aligned}$$

Here (i) follows from Cauchy-Schwarz, (ii) is a consequence of (185), Lemma 16 and the bound (87), and the last inequality holds as long as $m\gg\mu^2K\log^6 m$ and $C_3\ge 11C_1$.

- **Step 3(d): incoherence of the leave-one-out iterate $\boldsymbol{h}^{t+1}$ w.r.t. $\{\boldsymbol{b}_l\}$.** It remains to justify that $\boldsymbol{h}^{t+1}$ is also incoherent w.r.t. its associated design vectors $\{\boldsymbol{b}_l\}$. This proof of this step, however, is much more convoluted and challenging, due to the deterministic nature of the $\boldsymbol{b}_l$'s. As a result, we would need to "propagate" the randomness brought about by $\{\boldsymbol{a}_l\}$ to $\boldsymbol{h}^{t+1}$ in order to facilitate analysis. The result is summarized as follows.

  Lemma 17. *Suppose the inductive hypotheses (86a)-(86d) hold true for the tth iteration and the sample complexity obeys $m\gg\mu^2K\log^8 m$. Then with probability exceeding $1-O\left(m^{-10}\right)$,*

  $$\max_{1\le j\le m}\left|\boldsymbol{b}_j^*\tilde{\boldsymbol{h}}^{t+1}\right|\le C_4\frac{\mu}{\sqrt{m}}\log^2 m$$

  as long as C_4 is sufficiently large, and $\eta>0$ is taken to be some sufficiently small constant.

  Proof. The key idea is to divide $\{1,\cdots,m\}$ into consecutive bins each of size poly $\log(m)$, and to exploit the randomness (namely, the randomness from $\boldsymbol{a}_l$) within each bin altogether. This binning idea is crucial in ensuring that the incoherence measure of interest does not blow up in t. See Appendix C.4. □

With these steps in place, we conclude the proof of Theorem 3 via induction and the union bound.

8.5 The base case

In order to finish the induction steps, we still need to justify the induction hypotheses for the base cases, namely, we need to show that the spectral initializations $\boldsymbol{z}^0$ and $\left\{\boldsymbol{z}^{0,(l)}\right\}$ satisfy the induction hypotheses (86) with $t=0$. As usual, we will denote

$$\tilde{\boldsymbol{h}}^0:=\frac{1}{\overline{\alpha^0}}\boldsymbol{h}^0 \qquad \text{and} \qquad \tilde{\boldsymbol{x}}^0:=\alpha^0\boldsymbol{x}^0$$

with

$$\alpha^0:=\arg\min_{\alpha\in\mathbb{C}}\left\|\frac{1}{\overline{\alpha}}\boldsymbol{h}^0-\boldsymbol{h}^\natural\right\|_2^2+\left\|\alpha\boldsymbol{x}^0-\boldsymbol{x}^\natural\right\|_2^2. \tag{88}$$

To start with, the initialization is sufficiently close to the truth when measured by the ℓ_2 norm, as summarized by the following lemma.

Lemma 18. *With probability at least $1-O(m^{-10})$, there exists some constant $C>0$ such that*

$$\min_{\alpha\in\mathbb{C},|\alpha|=1}\left\{\left\|\alpha\boldsymbol{h}^0-\boldsymbol{h}^\natural\right\|_2+\left\|\alpha\boldsymbol{x}^0-\boldsymbol{x}^\natural\right\|_2\right\}\le\xi \qquad \textit{and} \tag{89}$$

$$\min_{\alpha\in\mathbb{C},|\alpha|=1}\left\{\left\|\alpha\boldsymbol{h}^{0,(l)}-\boldsymbol{h}^\natural\right\|_2+\left\|\alpha\boldsymbol{x}^{0,(l)}-\boldsymbol{x}^\natural\right\|_2\right\}\le\xi, \qquad 1\le l\le m, \tag{90}$$

provided that

$$m\ge\frac{C\mu^2K\log^2 m}{\xi^2}.$$

Proof. This follows from Wedin's sinΘ theorem [Wed72]. See Appendix C.5. □

By the definition of $\mathrm{dist}(\cdot,\cdot)$ (cf. (32)), we immediately have

$$\mathrm{dist}\big(\boldsymbol{z}^0,\boldsymbol{z}^\natural\big)=\min_{\alpha\in\mathbb{C}}\sqrt{\left\|\frac{1}{\overline{\alpha}}\boldsymbol{h}-\boldsymbol{h}^\natural\right\|_2^2+\left\|\alpha\boldsymbol{x}-\boldsymbol{x}^\natural\right\|_2^2}\overset{\text{(i)}}{\leq}\min_{\alpha\in\mathbb{C}}\left\{\left\|\frac{1}{\overline{\alpha}}\boldsymbol{h}-\boldsymbol{h}^\natural\right\|_2+\left\|\alpha\boldsymbol{x}-\boldsymbol{x}^\natural\right\|_2\right\}$$
$$\overset{\text{(ii)}}{\leq}\min_{\alpha\in\mathbb{C},|\alpha|=1}\left\{\left\|\alpha\boldsymbol{h}^0-\boldsymbol{h}^\natural\right\|_2+\left\|\alpha\boldsymbol{x}^0-\boldsymbol{x}^\natural\right\|_2\right\}\overset{\text{(iii)}}{\leq}C_1\frac{1}{\log^2 m},\tag{91}$$

as long as

$$m\geq C\mu^2K\log^6 m$$

for some sufficiently large constant $C>0$. Here (i) follows from the elementary inequality that $a^2+b^2\leq(a+b)^2$ for positive a and b, (ii) holds since the feasible set of the latter one is strictly smaller, and (iii) follows directly from Lemma 18. This finishes the proof of (86a) for $t=0$. Similarly, with high probability we have

$$\mathrm{dist}\big(\boldsymbol{z}^{0,(l)},\boldsymbol{z}^\natural\big)\leq\min_{\alpha\in\mathbb{C},|\alpha|=1}\left\{\left\|\alpha\boldsymbol{h}^{0,(l)}-\boldsymbol{h}^\natural\right\|_2+\left\|\alpha\boldsymbol{x}^{0,(l)}-\boldsymbol{x}^\natural\right\|_2\right\}\lesssim\frac{1}{\log^2 m},\quad 1\leq l\leq m.\tag{92}$$

Next, when properly aligned, the true initial estimate $(\boldsymbol{h}^0,\boldsymbol{x}^0)$ and the leave-one-out estimate $(\boldsymbol{h}^{0,(l)},\boldsymbol{x}^{0,(l)})$ are expected to be sufficiently close, as claimed by the following lemma. Along the way, we show that $\boldsymbol{h}^0$ is incoherent w.r.t. the sampling vectors $\{\boldsymbol{b}_j\}_{1\leq j\leq m}$. This estalibshes (86b) and (86d) for $t=0$.

***Lemma* 19.** *Suppose that $m\gg\mu^2K\log^3 m$. Then with probability at least $1-O(m^{-10})$,*

$$\mathrm{dist}\big(\boldsymbol{z}^{0,(l)},\tilde{\boldsymbol{z}}^0\big)\leq C_2\frac{\mu}{\sqrt{m}}\sqrt{\frac{\mu^2K\log^5 m}{m}}\tag{93}$$

and

$$\left|\boldsymbol{b}_l^*\tilde{\boldsymbol{h}}^0\right|\leq C_4\frac{\mu\log^2 m}{\sqrt{m}}.\tag{94}$$

Proof. The key is to establish that $\mathrm{dist}\big(\boldsymbol{z}^{0,(l)},\tilde{\boldsymbol{z}}^0\big)$ can be upper bounded by some linear scaling of $\left|\boldsymbol{b}_l^*\tilde{\boldsymbol{h}}^0\right|$, and vice versa. This allows us to derive bounds simultaneously for both quantities. See Appendix C.6. □

Finally, we establish (86c) regarding the incoherence of $\boldsymbol{x}^0$ with respect to the design vectors $\{\boldsymbol{a}_l\}_{1\leq l\leq m}$.

***Lemma* 20.** *Suppose that $m\gg\mu^2K\log^6 m$. Then with probability exceeding $1-O(m^{-10})$,*

$$\max_{1\leq l\leq m}\left|\boldsymbol{a}_l^*\big(\tilde{\boldsymbol{x}}^0-\boldsymbol{x}^\natural\big)\right|\leq C_3\frac{1}{\log^{1.5} m}.$$

Proof. See Appendix C.7. □

9 Discussions

This paper showcases an important phenomenon in nonconvex optimization: even without explicit enforcement of regularization, the vanilla form of gradient descent effectively achieves implicit regularization for a large family of statistical estimation problems. We believe this phenomenon arises in problems far beyond the three cases studied herein, and our results are initial steps towards understanding this fundamental phenomenon. That being said, there are numerous avenues open for future investigation, and we conclude the paper with a few of them.

- *Improving sample complexity.* In the current paper, the required sample complexity $O\left(\mu^3 r^3 n \log^3 n\right)$ for matrix completion is sub-optimal when the rank r of the underlying matrix is large. While this allows us to achieve a dimension-free iteration complexity, it is slightly higher than the one derived for regularized gradient descent in [CW15]. We expect our results continue to hold under lower sample complexity $O\left(\mu^2 r^2 n \log n\right)$, but it calls for a more refined analysis (e.g. a generic chaining argument).

- *Leave-one-out tricks for more general designs.* So far our focus is on independent designs, including the i.i.d. Gaussian design adopted in phase retrieval and partially in blind deconvolution, as well as the independent sampling mechanism in matrix completion. Such independence property creates some sort of "statistical homogeneity", for which the leave-one-out argument works beautifully. It remains unclear how to generalize such leave-one-out tricks for more general designs (e.g. more general sampling patterns in matrix completion and more structured Fourier designs in phase retrieval and blind deconvolution). In fact, the reader can already get a flavor of this issue in the analysis of blind deconvolution, where the Fourier design vectors require much more delicate treatments than for purely Gaussian designs.

- *Uniform stability.* The leave-one-out perturbation argument is established upon a basic fact: when we exclude one sample from consideration, the resulting estimates/predictions do not deviate much from the original ones. This leave-one-out stability bears similarity to the notion of uniform stability studied in learning theory [BE02, LLNT17]. We expect our analysis framework to be helpful for analyzing other learning algorithms that are uniformly stable.

- *Constrained optimization.* We restrict ourselves to study empirical risk minimization problems in an unconstrained setting. It will be interesting to explore if such implicit regularization still holds for constrained nonconvex problems.

- *Other iterative methods (e.g. mirror descent and alternating minimization).* Iterative methods other than gradient descent have been extensively studied in the nonconvex optimization literature, including alternating minimization, proximal methods, etc. Identifying the implicit regularization feature for a broader class of iterative algorithms is another direction worth exploring.

- *Connections to deep learning?* We have focused on nonlinear systems that are bilinear or quadratic in this paper. Deep learning formulations/architectures are notorious for its daunting nonconvex geometry. However, iterative methods including stochastic gradient descent have enjoyed enormous practical success in learning neural networks (e.g. [ZSJ+17, SJL17]), even when the architecture is significantly over-parameterized without explicit regularization. We hope the message conveyed in this paper for several simple statistical models can shed light on why simple forms of gradient descent and variants work so well in learning complicated neural networks.

Acknowledgements

The work of Y. Chi is supported in part by the grants AFOSR FA9550-15-1-0205, ONR N00014-15-1-2387, NSF CCF-1527456, ECCS-1650449 and CCF-1704245. Y. Chen would like to thank Yudong Chen for inspiring discussions about matrix completion.

References

[AAH17] A. Aghasi, A. Ahmed, and P. Hand. Branchhull: Convex bilinear inversion from the entrywise product of signals with known signs. *arXiv preprint arXiv:1702.04342*, 2017.

[AFWZ17] E. Abbe, J. Fan, K. Wang, and Y. Zhong. Entrywise eigenvector analysis of random matrices with low expected rank. *arXiv preprint arXiv:1709.09565*, 2017.

[ARR14] A. Ahmed, B. Recht, and J. Romberg. Blind deconvolution using convex programming. *IEEE Transactions on Information Theory*, 60(3):1711–1732, 2014.

[AS08] N. Alon and J. H. Spencer. *The Probabilistic Method (3rd Edition)*. Wiley, 2008.

[B+15] S. Bubeck et al. Convex optimization: Algorithms and complexity. *Foundations and Trends® in Machine Learning*, 8(3-4):231–357, 2015.

[BE02] O. Bousquet and A. Elisseeff. Stability and generalization. *Journal of Machine Learning Research*, 2(Mar):499–526, 2002.

[BEB17] T. Bendory, Y. C. Eldar, and N. Boumal. Non-convex phase retrieval from STFT measurements. *IEEE Transactions on Information Theory*, 2017.

[BNS16] S. Bhojanapalli, B. Neyshabur, and N. Srebro. Global optimality of local search for low rank matrix recovery. In *Advances in Neural Information Processing Systems*, pages 3873–3881, 2016.

[BR16] S. Bahmani and J. Romberg. Phase retrieval meets statistical learning theory: A flexible convex relaxation. *arXiv preprint arXiv:1610.04210*, 2016.

[CC16] Y. Chen and E. Candes. The projected power method: An efficient algorithm for joint alignment from pairwise differences. *arXiv preprint arXiv:1609.05820*, 2016.

[CC17] Y. Chen and E. J. Candès. Solving random quadratic systems of equations is nearly as easy as solving linear systems. *Comm. Pure Appl. Math.*, 70(5):822–883, 2017.

[CCG15] Y. Chen, Y. Chi, and A. J. Goldsmith. Exact and stable covariance estimation from quadratic sampling via convex programming. *IEEE Transactions on Information Theory*, 61(7):4034–4059, 2015.

[CESV13] E. J. Candès, Y. C. Eldar, T. Strohmer, and V. Voroninski. Phase retrieval via matrix completion. *SIAM Journal on Imaging Sciences*, 6(1):199–225, 2013.

[CFL15] P. Chen, A. Fannjiang, and G.-R. Liu. Phase retrieval with one or two diffraction patterns by alternating projections with the null initialization. *Journal of Fourier Analysis and Applications*, pages 1–40, 2015.

[CFMW17] Y. Chen, J. Fan, C. Ma, and K. Wang. Spectral method and regularized MLE are both optimal for top-k ranking. *arXiv preprint arXiv:1707.09971*, 2017.

[Che15] Y. Chen. Incoherence-optimal matrix completion. *IEEE Transactions on Information Theory*, 61(5):2909–2923, 2015.

[Che17] Y. Chen. Regularized mirror descent: A nonconvex approach for learning mixed probability distributions. 2017.

[Chi16] Y. Chi. Guaranteed blind sparse spikes deconvolution via lifting and convex optimization. *IEEE Journal of Selected Topics in Signal Processing*, 10(4):782–794, 2016.

[CJ16] V. Cambareri and L. Jacques. A non-convex blind calibration method for randomised sensing strategies. *arXiv preprint arXiv:1605.02615*, 2016.

[CJN17] Y. Cherapanamjeri, P. Jain, and P. Netrapalli. Thresholding based outlier robust pca. In *Conference on Learning Theory*, pages 593–628, 2017.

[CL14] E. J. Candès and X. Li. Solving quadratic equations via PhaseLift when there are about as many equations as unknowns. *Foundations of Computational Mathematics*, 14(5):1017–1026, 2014.

[CL16] Y. Chi and Y. M. Lu. Kaczmarz method for solving quadratic equations. *IEEE Signal Processing Letters*, 23(9):1183–1187, 2016.

[CLM+16] T. T. Cai, X. Li, Z. Ma, et al. Optimal rates of convergence for noisy sparse phase retrieval via thresholded Wirtinger flow. *The Annals of Statistics*, 44(5):2221–2251, 2016.

[CLMW11] E. J. Candès, X. Li, Y. Ma, and J. Wright. Robust principal component analysis? *Journal of ACM*, 58(3):11:1–11:37, Jun 2011.

[CLS15] E. J. Candès, X. Li, and M. Soltanolkotabi. Phase retrieval via Wirtinger flow: Theory and algorithms. *IEEE Transactions on Information Theory*, 61(4):1985–2007, April 2015.

[CLW17] J.-F. Cai, H. Liu, and Y. Wang. Fast rank one alternating minimization algorithm for phase retrieval. *arXiv preprint arXiv:1708.08751*, 2017.

[CR09] E. J. Candès and B. Recht. Exact matrix completion via convex optimization. *Foundations of Computational Mathematics*, 9(6):717–772, April 2009.

[CSPW11] V. Chandrasekaran, S. Sanghavi, P. A. Parrilo, and A. S. Willsky. Rank-sparsity incoherence for matrix decomposition. *SIAM Journal on Optimization*, 21(2):572–596, 2011.

[CSV13] E. J. Candès, T. Strohmer, and V. Voroninski. Phaselift: Exact and stable signal recovery from magnitude measurements via convex programming. *Communications on Pure and Applied Mathematics*, 66(8):1017–1026, 2013.

[CT10] E. Candès and T. Tao. The power of convex relaxation: Near-optimal matrix completion. *IEEE Transactions on Information Theory*, 56(5):2053 –2080, May 2010.

[CW15] Y. Chen and M. J. Wainwright. Fast low-rank estimation by projected gradient descent: General statistical and algorithmic guarantees. *arXiv preprint arXiv:1509.03025*, 2015.

[CYC14] Y. Chen, X. Yi, and C. Caramanis. A convex formulation for mixed regression with two components: Minimax optimal rates. In *Conf. on Learning Theory*, 2014.

[CZ15] T. Cai and A. Zhang. ROP: Matrix recovery via rank-one projections. *The Annals of Statistics*, 43(1):102–138, 2015.

[DK70] C. Davis and W. M. Kahan. The rotation of eigenvectors by a perturbation. iii. *SIAM Journal on Numerical Analysis*, 7(1):1–46, 1970.

[Dop00] F. M. Dopico. A note on $\sin\Theta$ theorems for singular subspace variations. *BIT*, 40(2):395–403, 2000.

[DR17] J. C. Duchi and F. Ruan. Solving (most) of a set of quadratic equalities: Composite optimization for robust phase retrieval. *arXiv preprint arXiv:1705.02356*, 2017.

[DTL17] O. Dhifallah, C. Thrampoulidis, and Y. M. Lu. Phase retrieval via linear programming: Fundamental limits and algorithmic improvements. *arXiv preprint arXiv:1710.05234*, 2017.

[EK15] N. El Karoui. On the impact of predictor geometry on the performance on high-dimensional ridge-regularized generalized robust regression estimators. *Probability Theory and Related Fields*, pages 1–81, 2015.

[EKBB+13] N. El Karoui, D. Bean, P. J. Bickel, C. Lim, and B. Yu. On robust regression with high-dimensional predictors. *Proceedings of the National Academy of Sciences*, 110(36):14557–14562, 2013.

[FWWZ17] J. Fan, D. Wang, K. Wang, and Z. Zhu. Distributed estimation of principal eigenspaces. *arXiv preprint arXiv:1702.06488*, 2017.

[GLM16] R. Ge, J. D. Lee, and T. Ma. Matrix completion has no spurious local minimum. In *Advances in Neural Information Processing Systems*, pages 2973–2981, 2016.

[GM17] R. Ge and T. Ma. On the optimization landscape of tensor decompositions. *arXiv preprint arXiv:1706.05598*, 2017.

[Gro11] D. Gross. Recovering low-rank matrices from few coefficients in any basis. *IEEE Transactions on Information Theory*, 57(3):1548–1566, March 2011.

[GS16] T. Goldstein and C. Studer. Phasemax: Convex phase retrieval via basis pursuit. *arXiv preprint arXiv:1610.07531*, 2016.

[GWB+17] S. Gunasekar, B. Woodworth, S. Bhojanapalli, B. Neyshabur, and N. Srebro. Implicit regularization in matrix factorization. *arXiv preprint arXiv:1705.09280*, 2017.

[GX16] B. Gao and Z. Xu. Phase retrieval using gauss-newton method. *arXiv preprint arXiv:1606.08135*, 2016.

[HH17] W. Huang and P. Hand. Blind deconvolution by a steepest descent algorithm on a quotient manifold. *arXiv preprint arXiv:1710.03309*, 2017.

[HKZ12] D. Hsu, S. M. Kakade, and T. Zhang. A tail inequality for quadratic forms of subgaussian random vectors. *Electron. Commun. Probab.*, 17:no. 52, 6, 2012.

[HMLZ15] T. Hastie, R. Mazumder, J. D. Lee, and R. Zadeh. Matrix completion and low-rank SVD via fast alternating least squares. *Journal of Machine Learning Research*, 16:3367–3402, 2015.

[HV16] P. Hand and V. Voroninski. An elementary proof of convex phase retrieval in the natural parameter space via the linear program PhaseMax. *arXiv preprint arXiv:1611.03935*, 2016.

[HW14] M. Hardt and M. Wootters. Fast matrix completion without the condition number. *Conference on Learning Theory*, pages 638 – 678, 2014.

[JEH15] K. Jaganathan, Y. C. Eldar, and B. Hassibi. Phase retrieval: An overview of recent developments. *arXiv preprint arXiv:1510.07713*, 2015.

[JKN16] C. Jin, S. M. Kakade, and P. Netrapalli. Provable efficient online matrix completion via nonconvex stochastic gradient descent. In *Advances in Neural Information Processing Systems*, pages 4520–4528, 2016.

[JM15] A. Javanmard and A. Montanari. De-biasing the lasso: Optimal sample size for gaussian designs. *arXiv preprint arXiv:1508.02757*, 2015.

[JN15] P. Jain and P. Netrapalli. Fast exact matrix completion with finite samples. In *Conference on Learning Theory*, pages 1007–1034, 2015.

[JNS13] P. Jain, P. Netrapalli, and S. Sanghavi. Low-rank matrix completion using alternating minimization. In *ACM symposium on Theory of computing*, pages 665–674, 2013.

[KD09] K. Kreutz-Delgado. The complex gradient operator and the cr-calculus. *arXiv preprint arXiv:0906.4835*, 2009.

[KLT11] V. Koltchinskii, K. Lounici, and A. B. Tsybakov. Nuclear-norm penalization and optimal rates for noisy low-rank matrix completion. *Ann. Statist.*, 39(5):2302–2329, 2011.

[KMN+16] N. S. Keskar, D. Mudigere, J. Nocedal, M. Smelyanskiy, and P. T. P. Tang. On large-batch training for deep learning: Generalization gap and sharp minima. *arXiv preprint arXiv:1609.04836*, 2016.

[KMO10a] R. H. Keshavan, A. Montanari, and S. Oh. Matrix completion from a few entries. *IEEE Transactions on Information Theory*, 56(6):2980 –2998, June 2010.

[KMO10b] R. H. Keshavan, A. Montanari, and S. Oh. Matrix completion from noisy entries. *J. Mach. Learn. Res.*, 11:2057–2078, 2010.

[KÖ16] R. Kolte and A. Özgür. Phase retrieval via incremental truncated Wirtinger flow. *arXiv preprint arXiv:1606.03196*, 2016.

[Kol11] V. Koltchinskii. *Oracle inequalities in empirical risk minimization and sparse recovery problems*, volume 2033 of *Lecture Notes in Mathematics*. Springer, Heidelberg, 2011. Lectures from the 38th Probability Summer School held in Saint-Flour, 2008, École d'Été de Probabilités de Saint-Flour. [Saint-Flour Probability Summer School].

[Lan93] S. Lang. Real and functional analysis. *Springer-Verlag, New York,*, 10:11–13, 1993.

[LB10] K. Lee and Y. Bresler. Admira: Atomic decomposition for minimum rank approximation. *IEEE Transactions on Information Theory*, 56(9):4402–4416, 2010.

[LCR16] J. Lin, R. Camoriano, and L. Rosasco. Generalization properties and implicit regularization for multiple passes SGM. In *International Conference on Machine Learning*, pages 2340–2348, 2016.

[LL17] Y. M. Lu and G. Li. Phase transitions of spectral initialization for high-dimensional nonconvex estimation. *arXiv preprint arXiv:1702.06435*, 2017.

[LLB17] Y. Li, K. Lee, and Y. Bresler. Blind gain and phase calibration for low-dimensional or sparse signal sensing via power iteration. In *Sampling Theory and Applications (SampTA), 2017 International Conference on*, pages 119–123. IEEE, 2017.

[LLJB17] K. Lee, Y. Li, M. Junge, and Y. Bresler. Blind recovery of sparse signals from subsampled convolution. *IEEE Transactions on Information Theory*, 63(2):802–821, 2017.

[LLNT17] T. Liu, G. Lugosi, G. Neu, and D. Tao. Algorithmic stability and hypothesis complexity. *arXiv preprint arXiv:1702.08712*, 2017.

[LLSW16] X. Li, S. Ling, T. Strohmer, and K. Wei. Rapid, robust, and reliable blind deconvolution via nonconvex optimization. *CoRR*, abs/1606.04933, 2016.

[LS15] S. Ling and T. Strohmer. Self-calibration and biconvex compressive sensing. *Inverse Problems*, 31(11):115002, 2015.

[LS17] S. Ling and T. Strohmer. Regularized gradient descent: A nonconvex recipe for fast joint blind deconvolution and demixing. *arXiv preprint arXiv:1703.08642*, 2017.

[LT16] Q. Li and G. Tang. The nonconvex geometry of low-rank matrix optimizations with general objective functions. *arXiv preprint arXiv:1611.03060*, 2016.

[LTR16] K. Lee, N. Tian, and J. Romberg. Fast and guaranteed blind multichannel deconvolution under a bilinear system model. *arXiv preprint arXiv:1610.06469*, 2016.

[LWL+16] X. Li, Z. Wang, J. Lu, R. Arora, J. Haupt, H. Liu, and T. Zhao. Symmetry, saddle points, and global geometry of nonconvex matrix factorization. *arXiv preprint arXiv:1612.09296*, 2016.

[Mat90] R. Mathias. The spectral norm of a nonnegative matrix. *Linear Algebra Appl.*, 139:269–284, 1990.

[Mat93] R. Mathias. Perturbation bounds for the polar decomposition. *SIAM Journal on Matrix Analysis and Applications*, 14(2):588–597, 1993.

[MBM16] S. Mei, Y. Bai, and A. Montanari. The landscape of empirical risk for non-convex losses. *arXiv preprint arXiv:1607.06534*, 2016.

[MM17] M. Mondelli and A. Montanari. Fundamental limits of weak recovery with applications to phase retrieval. *arXiv preprint arXiv:1708.05932*, 2017.

[MZL17] T. Maunu, T. Zhang, and G. Lerman. A well-tempered landscape for non-convex robust subspace recovery. *arXiv preprint arXiv:1706.03896*, 2017.

[NJS13] P. Netrapalli, P. Jain, and S. Sanghavi. Phase retrieval using alternating minimization. *Advances in Neural Information Processing Systems (NIPS)*, 2013.

[NNS+14] P. Netrapalli, U. Niranjan, S. Sanghavi, A. Anandkumar, and P. Jain. Non-convex robust PCA. In *Advances in Neural Information Processing Systems*, pages 1107–1115, 2014.

[NTS14] B. Neyshabur, R. Tomioka, and N. Srebro. In search of the real inductive bias: On the role of implicit regularization in deep learning. *arXiv preprint arXiv:1412.6614*, 2014.

[NTSS17] B. Neyshabur, R. Tomioka, R. Salakhutdinov, and N. Srebro. Geometry of optimization and implicit regularization in deep learning. *arXiv preprint arXiv:1705.03071*, 2017.

[NW12] S. Negahban and M. J. Wainwright. Restricted strong convexity and weighted matrix completion: optimal bounds with noise. *J. Mach. Learn. Res.*, 13:1665–1697, 2012.

[PKCS16] D. Park, A. Kyrillidis, C. Caramanis, and S. Sanghavi. Non-square matrix sensing without spurious local minima via the burer-monteiro approach. *arXiv preprint arXiv:1609.03240*, 2016.

[QZEW17] Q. Qing, Y. Zhang, Y. Eldar, and J. Wright. Convolutional phase retrieval via gradient descent. *Neural Information Processing Systems*, 2017.

[Rec11] B. Recht. A simpler approach to matrix completion. *Journal of Machine Learning Research*, 12(Dec):3413–3430, 2011.

[RFP10] B. Recht, M. Fazel, and P. A. Parrilo. Guaranteed minimum-rank solutions of linear matrix equations via nuclear norm minimization. *SIAM Review*, 52(3):471–501, 2010.

[SBE14] Y. Shechtman, A. Beck, and Y. C. Eldar. GESPAR: Efficient phase retrieval of sparse signals. *IEEE Transactions on Signal Processing*, 62(4):928–938, 2014.

[SCC17] P. Sur, Y. Chen, and E. J. Candès. The likelihood ratio test in high-dimensional logistic regression is asymptotically a rescaled chi-square. *arXiv preprint arXiv:1706.01191*, 2017.

[Sch92] B. A. Schmitt. Perturbation bounds for matrix square roots and Pythagorean sums. *Linear Algebra Appl.*, 174:215–227, 1992.

[SESS11] Y. Shechtman, Y. C. Eldar, A. Szameit, and M. Segev. Sparsity based sub-wavelength imaging with partially incoherent light via quadratic compressed sensing. *Optics express*, 19(16), 2011.

[SHS17] D. Soudry, E. Hoffer, and N. Srebro. The implicit bias of gradient descent on separable data. *arXiv preprint arXiv:1710.10345*, 2017.

[SJL17] M. Soltanolkotabi, A. Javanmard, and J. D. Lee. Theoretical insights into the optimization landscape of over-parameterized shallow neural networks. *arXiv preprint arXiv:1707.04926*, 2017.

[SL16] R. Sun and Z.-Q. Luo. Guaranteed matrix completion via non-convex factorization. *IEEE Transactions on Information Theory*, 62(11):6535–6579, 2016.

[Sol14] M. Soltanolkotabi. *Algorithms and Theory for Clustering and Nonconvex Quadratic Programming*. PhD thesis, Stanford University, 2014.

[Sol17] M. Soltanolkotabi. Structured signal recovery from quadratic measurements: Breaking sample complexity barriers via nonconvex optimization. *arXiv preprint arXiv:1702.06175*, 2017.

[SQW16] J. Sun, Q. Qu, and J. Wright. A geometric analysis of phase retrieval. In *Information Theory (ISIT), 2016 IEEE International Symposium on*, pages 2379–2383. IEEE, 2016.

[SQW17] J. Sun, Q. Qu, and J. Wright. Complete dictionary recovery over the sphere i: Overview and the geometric picture. *IEEE Transactions on Information Theory*, 63(2):853–884, 2017.

[SS12] W. Schudy and M. Sviridenko. Concentration and moment inequalities for polynomials of independent random variables. In *Proceedings of the Twenty-Third Annual ACM-SIAM Symposium on Discrete Algorithms*, pages 437–446. ACM, New York, 2012.

[Tao12] T. Tao. *Topics in Random Matrix Theory*. Graduate Studies in Mathematics. American Mathematical Society, Providence, Rhode Island, 2012.

[tB77] J. M. F. ten Berge. Orthogonal Procrustes rotation for two or more matrices. *Psychometrika*, 42(2):267–276, 1977.

[TBS+16] S. Tu, R. Boczar, M. Simchowitz, M. Soltanolkotabi, and B. Recht. Low-rank solutions of linear matrix equations via procrustes flow. In *Proceedings of the 33rd International Conference on International Conference on Machine Learning-Volume 48*, pages 964–973. JMLR. org, 2016.

[Tro15a] J. A. Tropp. Convex recovery of a structured signal from independent random linear measurements. In *Sampling Theory, a Renaissance*, pages 67–101. Springer, 2015.

[Tro15b] J. A. Tropp. An introduction to matrix concentration inequalities. *Found. Trends Mach. Learn.*, 8(1-2):1–230, May 2015.

[TV17] Y. S. Tan and R. Vershynin. Phase retrieval via randomized kaczmarz: Theoretical guarantees. *arXiv preprint arXiv:1706.09993*, 2017.

[TW16] J. Tanner and K. Wei. Low rank matrix completion by alternating steepest descent methods. *Applied and Computational Harmonic Analysis*, 40(2):417–429, 2016.

[Ver12] R. Vershynin. Introduction to the non-asymptotic analysis of random matrices. *Compressed Sensing, Theory and Applications*, pages 210 – 268, 2012.

[WCCL16] K. Wei, J.-F. Cai, T. F. Chan, and S. Leung. Guarantees of riemannian optimization for low rank matrix recovery. *SIAM Journal on Matrix Analysis and Applications*, 37(3):1198–1222, 2016.

[Wed72] P.-Å. Wedin. Perturbation bounds in connection with singular value decomposition. *BIT Numerical Mathematics*, 12(1):99–111, 1972.

[Wei15] K. Wei. Solving systems of phaseless equations via Kaczmarz methods: A proof of concept study. *Inverse Problems*, 31(12):125008, 2015.

[WGE17] G. Wang, G. B. Giannakis, and Y. C. Eldar. Solving systems of random quadratic equations via truncated amplitude flow. *IEEE Transactions on Information Theory*, 2017.

[WWS15] C. D. White, R. Ward, and S. Sanghavi. The local convexity of solving quadratic equations. *arXiv preprint arXiv:1506.07868*, 2015.

[WZG+16] G. Wang, L. Zhang, G. B. Giannakis, M. Akçakaya, and J. Chen. Sparse phase retrieval via truncated amplitude flow. *arXiv preprint arXiv:1611.07641*, 2016.

[YWS15] Y. Yu, T. Wang, and R. J. Samworth. A useful variant of the Davis-Kahan theorem for statisticians. *Biometrika*, 102(2):315–323, 2015.

[ZB17] Y. Zhong and N. Boumal. Near-optimal bounds for phase synchronization. *arXiv preprint arXiv:1703.06605*, 2017.

[ZBH+16] C. Zhang, S. Bengio, M. Hardt, B. Recht, and O. Vinyals. Understanding deep learning requires rethinking generalization. *arXiv preprint arXiv:1611.03530*, 2016.

[ZCL16] H. Zhang, Y. Chi, and Y. Liang. Provable non-convex phase retrieval with outliers: Median truncated Wirtinger flow. In *International conference on machine learning*, pages 1022–1031, 2016.

[ZL15] Q. Zheng and J. Lafferty. A convergent gradient descent algorithm for rank minimization and semidefinite programming from random linear measurements. In *Advances in Neural Information Processing Systems*, pages 109–117, 2015.

[ZL16] Q. Zheng and J. Lafferty. Convergence analysis for rectangular matrix completion using Burer-Monteiro factorization and gradient descent. *arXiv preprint arXiv:1605.07051*, 2016.

[ZLK+17] Y. Zhang, Y. Lau, H.-w. Kuo, S. Cheung, A. Pasupathy, and J. Wright. On the global geometry of sphere-constrained sparse blind deconvolution. In *Proceedings of the IEEE Conference on Computer Vision and Pattern Recognition*, pages 4894–4902, 2017.

[ZSJ+17] K. Zhong, Z. Song, P. Jain, P. L. Bartlett, and I. S. Dhillon. Recovery guarantees for one-hidden-layer neural networks. *arXiv preprint arXiv:1706.03175*, 2017.

[ZWL15] T. Zhao, Z. Wang, and H. Liu. A nonconvex optimization framework for low rank matrix estimation. In *Advances in Neural Information Processing Systems*, pages 559–567, 2015.

[ZZLC17] H. Zhang, Y. Zhou, Y. Liang, and Y. Chi. A nonconvex approach for phase retrieval: Reshaped wirtinger flow and incremental algorithms. *Journal of Machine Learning Research*, 2017.